Gas-Phase Oxidation and Nitration of First-, Second-, and Third-Row Atomic Cations in Reactions with Nitrous Oxide: Periodicities in Reactivity

Vitali V. Lavrov, Voislav Blagojevic, Gregory K. Koyanagi, Galina Orlova, and Diethard K. Bohme*

Department of Chemistry, Centre for Research in Mass Spectrometry and Centre for Research in Earth and Space Science, York University, Toronto, Ontario, Canada, M3J 1P3

Received: January 6, 2004; In Final Form: April 12, 2004

Room-temperature reactions of 46 different atomic cations with N_2O have been surveyed systematically using an inductively coupled plasma/selected-ion flow tube (ICP/SIFT) tandem mass spectrometer. The atomic cations are produced at about 5500 K in the ICP source and are allowed to decay radiatively and thermalize by collisions with Ar and He atoms prior to reaction. Rate coefficients were measured for the reactions of first-row atomic cations from K^+ to Se^+, of second-row atomic cations from Rb^+ to Te^+ (excluding Tc^+), and of third-row atomic cations from Cs^+ to Bi^+. Primary reaction channels were observed corresponding to O-atom transfer, N-atom transfer, and N_2O addition. Periodicities were observed in overall reaction efficiency, and these are scrutinized in terms of overall exothermicity, the presence of an activation barrier in the reaction coordinate, and the overall conservation of spin. N-atom transfer was observed to compete with O-atom transfer in the reactions of N_2O with La^+ (4%), Ti^+ (22%), Zr^+ (45%), Nb^+ (35%), Ta^+ (40%), and Os^+ (60%). Up to three N_2O molecules were observed to add sequentially to selected atomic cations as well as several monoxide and dioxide cations. A second O-atom transfer was observed with the group 4, 5, and 6 transition-metal ions (except Mo^+) as well as the third-row cations Re^+, Os^+, Ir^+, and Pt^+. The atomic ions W^+, Os^+, and Ir^+ formed trioxides in sequential O-atom transfer reactions, and Os^+ even formed the tetroxide OsO_4^+. Multicollision-induced dissociation studies with Ar buffer gas indicated thermodynamically controlled dissociation of TiO_2^+, ZrO_2^+, HfO_2^+, VO_2^+, NbO_2^+, TaO_2^+, and WO_2^+ by the consecutive detachment of O-atoms while CrO_2^+, ReO_2^+, and PtO_2^+ decomposed primarily by loss of O_2 molecules.

1. Introduction

Recent instrumental developments in our laboratory have provided the means to survey trends in chemical kinetics for reactions of atomic cations with gaseous molecules across and down the periodic table. For example, we have recently surveyed reactions of first-, second-, and third-row atomic cations with molecular oxygen, both in the absence and presence of benzene, and with hexafluorobenzene.[1] Here we report results obtained for reactions of atomic cations with nitrous oxide which can be important in atmospheric chemistry[2] and in biological metabolism.[3] The focus is on reactions of first-, second-, and third-row atomic cations; we have previously reported experimental results for the chemical kinetics of lanthanide cations reacting with N_2O.[4]

The study of the gas-phase atomic ion chemistry of nitrous oxide in the past in other laboratories has focused primarily on reactions with atomic transition-metal ions. In part this is because of the low O-atom affinity of N_2 for N_2O formation, $OA(N_2) = 40$ kcal mol^{-1},[5] which makes N_2O a useful O-atom donor for the production of transition-metal oxide cations.[6,7] Transition-metal oxide cations also are of interest as intermediates in transition-metal ion catalysis. For example, when reduced by CO to the metal cation and CO_2, the metal oxide cation can serve as a mediator in the catalytic reduction of N_2O by CO to N_2 and CO_2.[8,9] Others have examined the translational energy dependence of the cross sections for reactions of atomic metal ions with N_2O in part with a view to extracting bond energies for atomic metal oxide cations.[10]

Reactions of atomic cations with N_2O also provide a unique opportunity to assess fundamental aspects of chemical reactivity such as the role of spin conservation in determining reaction efficiency. Armentrout et al.[10] have pointed out the need for spin conservation in efficient reactions of atomic metal cations with N_2O. Also, the need for spin conservation will give rise to spin restrictions in the formation of metal oxide product ions so that formation of excited state products may be preferred. Spin restrictions have been carefully examined for the reactions reported here, also with a view to the initial electronic state of the reactant atomic ion.

The transition-metal ions employed in previous measurements of N_2O chemistry generally were produced by laser ablation/ionization techniques. In the experiments reported in this study atomic ions are generated in an inductively coupled plasma (ICP) of argon at 1 atm.[11] For the kinetic studies reported here the ICP was linked to a selected-ion flow tube (SIFT) tandem mass spectrometer. The ICP/SIFT combination provides an extremely versatile instrument for the measurement of the chemical kinetics of reactions of atomic ions and has been found to be suitable for virtually any element on the periodic table (with the exception of ions with a mass less than Ar).[11] In this study we examine the room-temperature chemistry and kinetics of ion−molecule reactions between nitrous oxide and atomic cations of all available transition elements and of many s and p elements and so the influence of the electronic configuration

* Corresponding author. E-mail: dkbohme@yorku.ca. Phone: 416-736-2100, ext 66188. Fax: 416-736-5936.

10.1021/jp049931d CCC: $27.50
Published on Web 06/08/2004

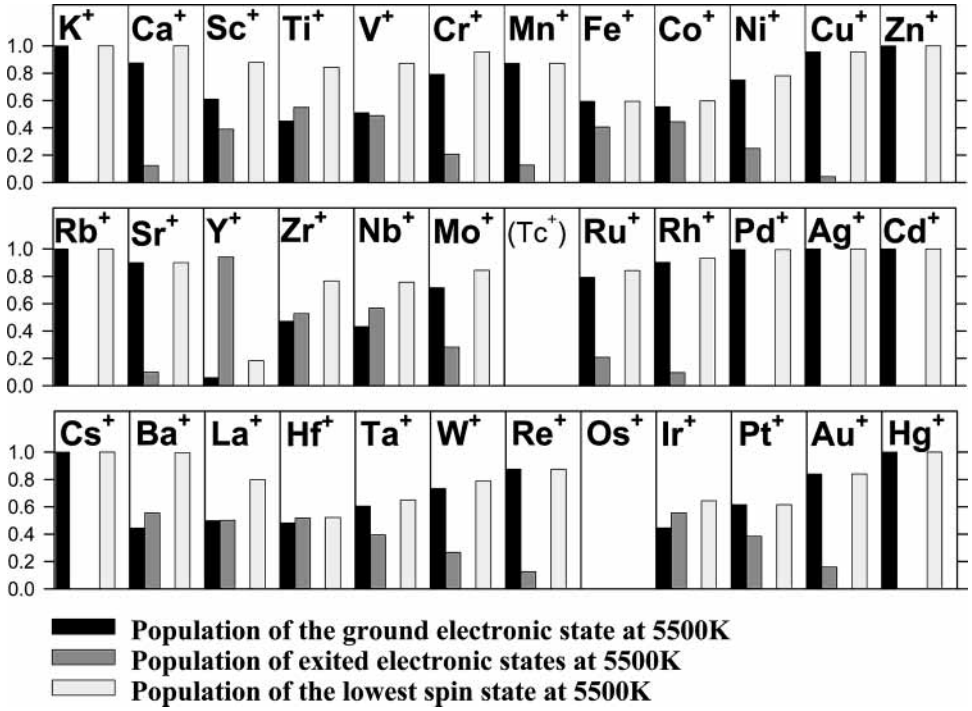

Figure 1. Bar graph showing computed populations based on spectroscopic data (see text and Tables 1 and 2) for the ground and excited (below 3.7 eV) electronic states of atomic cations generated in the ICP at a temperature of 5500 K. Also given is the total population of cations with the same spin state as the ground electronic state (viz. with the lowest spin state).

of an atomic cation in determining chemical reactivity. The gas-phase behavior reported here for what are bare, unligated atomic cations interacting with N_2O also may serve as a benchmark for the interactions of N_2O with metal cations ligated to small molecules or larger molecular frameworks such as those important in the biometallic chemistry of nitrous oxide[12] or in the catalytic reduction of nitrous oxide with metal-exchanged zeolites.[13]

2. Experimental Section

The results reported here were obtained using the ICP/SIFT/CID mass spectrometer. The apparatus has been described previously.[11] Elemental ions of interest are generated from the diluted solutions of salts containing the corresponding element by spraying them into an inductively coupled plasma (ICP) of argon with a nominal temperature of 5500 K which guarantees a significant degrees of atomization/ionization of these salts. The sample solutions were prepared using atomic spectroscopy standard solutions commercially available from SPEX, Teknolab, J. T. Baker Chemical Co., Fisher Scientific Company, Perkin-Elmer, and Alfa Products. Aliquots of standard solutions were diluted with highly purified water produced in the Millipore Milli-Qplus ultra-pure water system. The final concentrations were varied within a 5−20 ppm interval to achieve suitable intensity of the resultant ion beam. Normally, a stabilizing agent was added to each solution to prevent precipitation. That was either HNO_3 or HCl for acid-stabilized salts, and KOH for those that were base-stabilized.

The ions produced in the ICP were injected through a differentially pumped sampling interface into a quadrupole mass spectrometer and, after mass analysis, introduced through an aspirator-like interface into flowing helium carrier gas at 0.35 Torr and 295 ± 2 K. After experiencing about 10^5 collisions with He atoms, the ions were allowed to react with added nitrous oxide. The atomic ions emerging from the atmospheric-pressure plasma have a Boltzmann internal energy distribution characteristic of the plasma temperature and may experience both radiative electronic-state relaxation and collisional electronic-state relaxation. Atomic ions emerge from the ICP at a nominal ion temperature of 5500 K with the Boltzmann state distributions given in Tables 1 (transition-metal cations) and 2 (main group cations) and displayed in Figure 1. These distributions were derived from available optical spectra[14] and are given for the two electronic spin states with the highest population at 5500 K. Os^+ is not shown since no suitable spectroscopic data could be found. Energy levels as high as 3.7 eV (30 000 cm^{-1}) were included in the calculations. Table 1 shows that the state distributions are more variable for the transition-metal cations. Excited states contribute 20% or less toward the populations of Cr^+, Mn^+, Ni^+, Cu^+, Zn^+, Rh^+, Pd^+, Ag^+, Cd^+ Re^+, Au^+, and Hg^+ and 50% or more toward the populations of Ti^+, Y^+, Zr^+, Nb^+, La^+, and Ir^+ at 5500 K. Table 2 shows that excited states of the main group elements, except for Ba^+, are high in energy and contribute little (never more than 13%) to the total ion population at 5500 K.

Radiative electronic-state relaxation and collisional electronic-state relaxation with argon may occur as the extracted plasma cools upon sampling and then by collisions with He atoms in the flow tube (ca. 4×10^5 collisions) prior to the reaction region, but the actual extent of electronic relaxation (either radiative or collisional) is not known and is difficult to assess. Almost all of the electronic states of the transition-metal ions have positive parity; electric dipole transitions between states of the same parity are forbidden (Laporte rule[15]). This means that radiative transitions between different states in metal cations can be achieved only by either magnetic dipole or electric quadrupole radiation. The probabilities for these transitions are very low,[16] and the resulting radiative lifetimes are of the order of seconds or larger. The time interval in the ICP/SIFT experiments between the exit of the ICP source and the entrance in the reaction region is ∼20 ms, and therefore no major modification of state distributions can occur in this time interval

TABLE 1: Electronic-State Information and Population Distributions Calculated for Transition-Metal Cations at 5500 K[a]

ion	term	electron configuration	population (%)	energy range (eV)	number of levels[b]
Sc^+	^3D	$3d4s$	61.03	0.0−0.022	3
	^1F	$3d4s$	10.76	0.32	1
	^3F	$3d^2$	24.32	0.60−0.62	3
	^1D	$3d^2$	1.194	1.36	1
Ti^+	^4F	$3d^24s$	45.39	0.0−0.05	4
	^4F	$3d^3$	36.23	0.11−0.15	4
	^2F	$3d^24s$	6.89	0.57−0.61	2
	^2D	$3d^24s$	1.75	1.08−1.084	2
V^+	^5D	$3d^4$	51.03	0.0−0.042	5
	^5F	$3d^34s$	35.10	0.32−0.39	5
	^3F	$3d^{12345}4s^2$	4.41	1.07−1.13	3
Cr^+	^6S	$3d^5$	79.24	0.0	1
	^6D	$3d^44s$	15.98	1.48−1.55	5
Mn^+	^7S	$3d^54s$	87.23	0.0	1
	^5S	$3d^54s$	5.23	1.17	1
Fe^+	^6D	$3d^64s$	59.39	0.0−0.12	5
	^4F	$3d^7$	32.96	0.23−0.39	4
	^4D	$3d^64s$	5.03	0.99−1.10	4
Co^+	^3F	$3d^8$	55.51	0.0−0.20	3
	^5F	$3d^74s$	37.45	0.42−0.65	5
	^3F	$3d^74s$	4.30	1.22−1.40	3
Ni^+	^2D	$3d^9$	75.14	0.0−0.19	2
	^4F	$3d^84s$	21.43	1.04−1.32	4
Cu^+	^1S	$3d^{10}$	95.59	0.0	1
	^3D	$3d^94s$	3.91	2.72−2.98	3
Zn^+	^2S	$3d^{10}4s$	99.999	0.0	1
	$^2P°$	$3d^{10}4p$	0.001	6.01−6.12	2
Y^+	^1S	$5s^2$	5.90	0.0	1
	^3D	$4d5s$	64.86	0.10−0.18	3
	^1D	$4d5s$	12.45	0.41	1
	^3F	$4d^2$	13.69	0.99−1.08	3
Zr^+	^4F	$4d^25s$	47.16	0.0−0.16	4
	^4F	$4d^3$	24.39	0.32−0.47	4
	^2D	$4d^25s$	6.44	0.53−0.59	2
	^2P	$4d^25s$	2.56	0.71−0.76	2
	^2F	$4d^25s$	5.72	0.71−0.80	2
	^4P	$4d^25s$	3.13	0.93−1.00	3
Nb^+	^5D	$4d^4$	43.23	0.0−0.15	5
	^5F	$4d^35s$	30.68	0.29−0.51	5
	^3P	$4d^4$	3.31	0.69−0.90	3
	^3P	$4d^35s$	5.49	0.93−1.03	3
Mo^+	^6S	$4d^5$	71.68	0.0	1
	^6D	$4d^45s$	12.74	1.46−1.67	5
Tc^+	not available				
Ru^+	^4F	$4d^7$	79.17	0.0−0.39	4
	^4P	$4d^7$	5.08	1.02−1.16	3
Rh^+	^3F	$4d^8$	90.30	0.0−0.444	3
	^1D	$4d^8$	3.63	1.01	1
Pd^+	^2D	$4d^9$	99.62	0.0−0.44	2
	^4F	$4d^85s$	0.34	3.11−3.71	4
Ag^+	^1S	$4d^{10}$	99.96	0.0	1
	^3D	$4d^95s$	0.04	4.85−5.42	3
Cd^+	^2S	$5s$	99.998	0.0	1
	$^2P°$	$5p$	0.002	5.47−5.78	2
La^+	^3F	$5d^2$	49.82	0.0−0.24	3
	^1D	$5d6s$	10.99	0.17	1
	^3D	$5d6s$	23.28	0.24−0.40	3
	^3P	$5d^2$	6.03	0.65−0.77	3
	^1S	$6s^2$	0.46	0.77	1
	^1G	$5d^2$	4.03	0.92	1
	^1D	$5d^2$	1.13	1.25	1
Hf^+	^2D	$5d6s^2$	48.21	0.0−0.38	2
	^4F	$5d^26s$	42.07	0.45−1.04	4
Ta^+	^5F	$5d^36s$	60.45	0.0−0.77	5
	^3F	$5d^26s^2$	15.97	0.39−1.21	3
	^3P	$5d^26s^2$	8.76	0.51−0.70	3
W^+	^6D	$5d^46s$	73.42	0.0−0.762	5
	^6S	$5d^5$	5.43	0.92	1
	^4F	$5d^46s$	7.36	1.08−1.84	4
Re^+	^7S	$5d^56s$	87.86	0.0	1
	^5D	$5d^46s^2$	6.66	1.71−1.85	5
Os^+	not available				
Ir^{+c}	$^5F^d$	$5d^76s$	44.52	0.0	1
	$^3F^e$	$5d^8$	10.15	0.28	1
	$^3P^f$		9.02	0.38	1
	$^5F^g$		10.41	0.59	1
	$^5F^h$		3.33	1.02	1
Pt^+	^2D	$5d^9$	61.61	0.0−1.04	2
	^4F	$5d^86s$	36.33	0.59−1.96	4
Au^+	^1S	$5d^{10}$	83.98	0.0	1
	^3D	$5d^96s$	15.84	1.86−3.44	3
Hg^+	^2S	$5d^{10}6s$	99.97	0.0	1
	^2D	$5d^96s^2$	0.03	4.40−6.27	2

[a] States up to the first state at or above 1 eV were included in the calculations which were based on known optical spectra.[14] [b] Number of microstates within a specified electronic level. [c] Only mixed spin states could be specified.[15] [d] Actual configuration: 89% ^5F, 10% ^3G. [e] Actual configuration: 90% ^3F, 4% ^1G, 3% ^3F. [f] Actual configuration: 33% ^3P, 25% ^3P, 17% ^1D. [g] Actual configuration: 79% ^5F, 11% ^3F, 7% ^3G. [h] Actual configuration: 77% ^5F, 7% ^3F, 5% ^3D.

by forbidden radiative decay. The extent of electronic relaxation by collisions with the quite polarizable Ar atoms is uncertain and could be inferred only indirectly from the observed decays of primary ion signals and observed product ions. Collisions with Ar and He ensure that the atomic ions reach a translational temperature equal to the tube temperature of 295 ± 2 K prior to entering the reaction region. Similar conditions of Ar and He have been used by Zhang and Armentrout in their studies of atomic ions emerging from a direct-current discharge, and these authors have found that their atomic ions generally are produced in their ground electronic state, with the exception of Pt^+.[17]

Reactant and product ions were sampled still further downstream with a second quadrupole mass spectrometer and were

TABLE 2: Electronic-State Information and Population Distributions Calculated for Main Group Metal Cations at 5500 K[a]

ion	term	configuration	population (%)	energy range (eV)	number of levels[b]
K^+	^1S	$3p^6$	100.0	0.0	1
Ca^+	^2S	$3p^64s$	87.46	0.0	1
	^2D	$3p^63d$	12.19	1.69−1.70	2
Ga^+	^1S	$4s^2$	100.0	0.0	1
Ge^+	$^2P°$	$4s^24p$	100.0	0.0−0.22	2
As^+	^3P	$4s^24p^2$	94.21	0.0−0.32	3
	^1D	$4s^24p^2$	5.75	1.25	1
Se^+	$^4S°$	$4s^24p^3$	92.95	0.0	1
		$4s^24p^3$	6.75	1.63−1.71	2
Rb^+	^1S	$4p^6$	100.0	0.0	1
Sr^+	^2S	$4p^65s$	89.96	0.0	1
	^2D	$4p^64d$	9.56	1.80−1.84	2
In^+	^1S	$5s^2$	100.0	0.0	1
Sn^+	$^2P°$	$5s^25p$	100.0	0.0−0.53	2
Sb^+	^3P	$5s^25p^2$	95.14	0.0−0.70	3
	^1D	$5s^25p^2$	4.81	1.59	1
Te^+	$^4S°$	$5s^25p^3$	88.39	0.0	1
	$^2D°$	$5s^25p^3$	11.24	1.27−1.54	2
Cs^+	^1S	$5p^6$	100.0	0.0	1
Ba^+	^2S	$5p^66s$	44.44	0.0	1
	^2D	$5p^65d$	55.05	0.60−0.70	2
Tl^+	^1S	$6s^2$	100.0	0.0	1
Pb^+	$^2P°$	$6s^26p$	100.0	0.0−1.75	2
Bi^+	^3P	$6s^26p^2$	99.94	0.0−2.11	3
	^1D	$6s^26p^2$	0.06	4.21	1

[a] States up to the first state at or above 1 eV were included in the calculations which were based on known optical spectra.[14] [b] Number of microstates within a specified electronic level.

measured as a function of added reactant. The resulting profiles provide information about product-ion distribution, reaction rate coefficients, and reaction molecularity. Product-ion distributions and rate coefficients were obtained in the usual manner. Only very weakly bonded adducts (<3 or 4 kcal mol^{-1}) can dissociate under our sampling conditions. The dissociation energies of the N_2O adduct ions observed in this study are generally not known but are expected to be larger than 4 kcal mol^{-1} in view of the observation of higher-order adducts. This is the case for the two metal actions (Cr^+ and Co^+) for which adduct formation is observed to compete with O-atom transfer. Rate coefficients for the primary and higher-order reactions reported here have an absolute accuracy estimated to be better than ±30%.

Nitrous oxide was introduced into the reaction region of the SIFT either as a pure gas or as a dilute mixture in helium when the observed reaction was too fast to use pure reactant. The nitrous oxide was obtained commercially and was of high purity (Matheson Gas products, >98.0%). When rate coefficients are reported as an upper limit (≤), this indicates the statistical scatter in the data was significant compared to the slope of the data and an upper limit (based on the line of steepest slope through the data) is reported.

3. Results and Discussion

The reactions of 46 different atomic ions from the first, second, and third rows of the periodic table were investigated with N_2O at a helium buffer-gas pressure of 0.35 ± 0.01 Torr and temperature of 295 ± 2 K. Both the primary and higher-order chemistry was monitored. The primary reactions exhibited a wide range in reactivity with measured rate coefficients in the range from $<10^{-13}$ to 7.7×10^{-10} cm^3 $molecule^{-1}$ s^{-1}, and the three different channels indicated in reaction 1 were observed.

$$M^+ + N_2O \rightarrow MO^+ + N_2 \quad (1a)$$

$$\rightarrow MN^+ + NO \quad (1b)$$

$$\rightarrow M^+N_2O \quad (1c)$$

The bimolecular channels correspond to O-atom transfer (channel 1a) and N-atom transfer (channel 1b). The O-atom affinity of nitrogen to form nitrous oxide, $OA(N_2) = 39.95 \pm 0.02$ kcal mol^{-1}, while the N-atom affinity of NO to form nitrous oxide, $NA(NO) = 114.9 \pm 0.1$ kcal mol^{-1}.[5] Available O-atom and N-atom affinities (see Tables 3 and 4, respectively) indicate that O-atom transfer is exothermic with 32 of the 40 atomic ions for which O-atom affinities are known and N-atom transfer is exothermic with possibly 2 of the 7 atomic ions for which N-atom affinities are known from either experiment or theory (most N-atom affinities are not known).

TABLE 3: O-Atom Affinities, $D_0(M^+-O)$ in kcal mol^{-1}, and Ionization Energies, IE(M) in eV,[1] for First-, Second-, and Third-Row Atomic Cations[a]

first row			second row			third row		
M^+	$OA(M^+)$	IE(M)	M^+	$OA(M^+)$	IE(M)	M^+	$OA(M^+)$	IE(M)
K^+	3	4.34	Rb^+	7	4.18	Cs^+	14	3.89
Ca^+	77.2	6.11	Sr^+	71.4	5.70	Ba^+	92.8	5.21
Sc^+	164.6 ± 1.4[b]	6.56	Y^+	167.0 ± 4.2[c]	6.22	La^+	206 ± 4[e]	5.58
Ti^+	158.6 ± 1.6[b]	6.83	Zr^+	178.9 ± 2.5[c]	6.63	Hf^+	173 ± 5[f]	6.83
V^+	134.9 ± 3.5[b]	6.75	Nb^+	164.4 ± 2.5[c]	6.76	Ta^+	188 ± 15[f]	7.55
Cr^+	85.8 ± 2.8[b]	6.77	Mo^+	116.7 ± 0.5[c]	7.09	W^+	166 ± 10[g]	7.86
Mn^+	68.0 ± 3.0[b]	7.43	Tc^+			Re^+	115 ± 15[h]	7.83
Fe^+	80.0 ± 1.4[b]	7.90	Ru^+	87.9 ± 1.2[d]	7.36	Os^+	100 ± 12[i]	8.44
Co^+	74.9 ± 1.2[b]	7.88	Rh^+	69.6 ± 1.4[d]	7.46	Ir^+	59[f]	8.97
Ni^+	63.2 ± 1.2[b]	7.64	Pd^+	33.7 ± 2.5[d]	8.34	Pt^+	77[j]	8.96
Cu^+	37.4 ± 3.5[b]	7.72	Ag^+	28.4 ± 1.2[d]	7.58	Au^+		9.23
Zn^+	38.5 ± 1.2[b]	9.39	Cd^+		8.99	Hg^+		10.44
Ga^+	5.6	6.00	In^+		5.79	Tl^+		6.11
Ge^+	81.8	7.90	Sn^+	75.1	7.34	Pb^+	53.2	7.42
As^+	147 ± 2[k]	9.81	Sb^+		8.64	Bi^+	41.6	7.29
Se^+	92[k]	9.75	Te^+	96.6	9.01			

[a] With few exceptions, the values for OA were taken from the review of Schröder et al.[18] [b] Reference 19. [c] Reference 20. [d] Reference 21. [e] Reference 22. [f] Reference 5. [g] Reference 23. [h] Reference 24. [i] Reference 25. [j] Reference 26. [k] Reference 27.

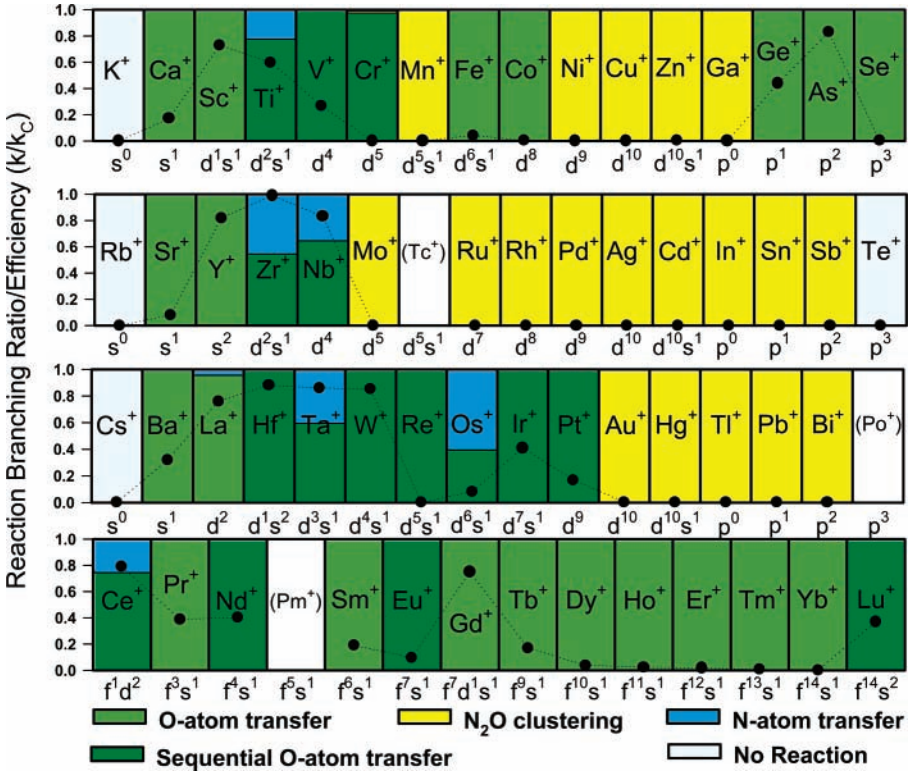

Figure 2. Periodic variations observed in the efficiencies, k/k_c (represented as solid circles), for reactions of atomic cations with nitrous oxide; k represents the measured reaction rate coefficient, and k_c is the calculated collision rate coefficient (see Table 5). Also indicated are the observed reaction channels and the ground-state electronic configurations of the atomic cations. The reactions of Tc^+ and Po^+ were not investigated. The results for the reactions of lanthanide cations have been reported previously.[2]

No other bimolecular channels were observed. Electron transfer is endothermic for all the atomic ions investigated since the ionization energy of N_2O is quite high, IE(N_2O) = 12.886 eV.[5] A total of 23 of the 46 reactions investigated exhibited one or more of the bimolecular channels 1a and 1b. The remaining 23 reactions were all quite slow ($k < 2.4 \times 10^{-12}$ cm^3 $molecule^{-1}$ s^{-1}). Nineteen of these were observed to proceed by addition (channel 1c) while the remaining four (K^+, Rb^+, Cs^+, and Te^+) showed no products at all in the flow regime investigated although they are expected to react by addition at higher flows. Only two atomic ions (Cr^+ and Co^+) were observed to proceed by both addition and one of the bimolecular channels. The addition is assumed to occur in a termolecular fashion with He acting as the third body; no attempt was made to measure the pressure dependence of this channel since a large range in pressure was not experimentally accessible.

Table 5 summarizes the rate coefficients, reaction efficiencies, and product distributions measured in this study. The reaction efficiency is taken to be equal to the ratio k/k_c, where k is the experimentally measured rate coefficient and k_c is the capture or collision rate coefficient computed using the algorithm of the modified variational transition-state/classical trajectory theory developed by Su and Chesnavich[37a] with a polarizability, $\alpha(N_2O)$ = 3.03 Å[3,37b] and dipole moment, μ_D = 0.167 D.[37c] Figure 2 displays these results on a periodic table. Figures 3, 4, and 5 display data obtained for selected ions in the first, second, and third rows of the periodic table, respectively.

3.1. First-Row Atomic Ions. With the exception of the nonreaction of K^+ and the N-atom transfer channel observed with Ti^+, only O-atom transfer and N_2O addition were observed as primary products for the first-row atomic ions. Secondary dioxide formation according to reaction 2 was observed for the early transition ions $M^+ = Ti^+$, V^+, and Cr^+, but not Sc^+:

TABLE 4: Nitrogen-Atom Affinities, NA, for Some Atomic Cations M^+ [a]

			experiment	theory
M^+	IE(MN)	D(M−N)	NA(M^+)[b]	NA(M^+)
Sc^+				63.1[j]
Ti^+	137 ± 50[c]	123[g]	143 ± 62 119.6 ± 3.0[h]	97.8[j]
V^+	182 ± 20[d]	116[g]	89 ± 42 107.2 ± 1.4[i]	87.1[j]
Cr^+				49.5[j]
Zr^+	180 ± 10[e]	135 ± 9[e]	113 ± 19	
Nb^+				134[k]
Hf^+	228[f]	141[g]	69 (± >12)	

[a] All values are in kcal mol^{-1}. [b] Unless indicated otherwise, derived using NA(M^+) = D(M−N) + IE(M) − IE(MN). Values for IE(M) and other supporting thermodynamics were taken from ref 5. [c] Reference 28. [d] Reference 29. [e] Reference 30. [f] Reference 31. [g] Reference 32. [h] Reference 33. [i] Reference 34. [j] Reference 35. [k] Reference 36.

$$MO^+ + N_2O \rightarrow MO_2^+ + N_2 \qquad (2)$$

Secondary and higher-order N_2O addition was observed for $M^+ = Cr^+$ (n = 1), Co^+ (n = 1,2), Ni^+ (n = 1,2) and Cu^+ (n = 1), $MO^+ = ScO^+$ (n = 0−2), CrO^+ (n = 0−2), FeO^+ (n = 0−2), CoO^+ (n = 0−2), GeO^+ (n = 0) and AsO^+ (n = 0) and $MO_2^+ = TiO_2^+$ (n = 0−2), VO_2^+ (n = 0−2), and CrO_2^+ (n = 0,1) cations according to reactions 3−5:

$$M^+(N_2O)_n + N_2O \rightarrow M^+(N_2O)_{n+1} \qquad (3)$$

$$MO^+(N_2O)_n + N_2O \rightarrow MO^+(N_2O)_{n+1} \qquad (4)$$

$$MO_2^+(N_2O)_n + N_2O \rightarrow MO_2^+(N_2O)_{n+1} \qquad (5)$$

TABLE 5: Rate Coefficients (in Units of cm^3 molecule^{-1} s^{-1}), Reaction Efficiencies (k/k_c), and Higher-Order Product Ions Measured for Reactions of Atomic Ions M^+ with Nitrous Oxide in Helium at 0.35 ± 0.01 Torr and 295 ± 2 K Ordered According to Row in the Periodic Table[a]

M^+	k [b]	k_c [c]	k/k_c	primary products	PD[d] (%)	higher-order product ions
K^+	$<10^{-13}$	9.3×10^{-10}	$<10^{-4}$			
Ca^+	1.6×10^{-10}	9.3×10^{-10}	0.17	CaO^+	100	
Sc^+	6.6×10^{-10}	9.0×10^{-10}	0.73	ScO^+	100	$ScO^+\cdot(N_2O)_n$, $n = 1-3$
Ti^+	5.3×10^{-10}	8.9×10^{-10}	0.60	TiO^+	78	$TiO_2^+\cdot(N_2O)_n$, $n = 0-3$
				TiN^+	22	
V^+	2.4×10^{-10}	8.8×10^{-10}	0.27	VO^+	100	$VO_2^+\cdot(N_2O)_n$, $n = 0-3$
Cr^+	1.5×10^{-13}	8.7×10^{-10}	0.00017	CrO^+	98	$CrO^+\cdot(N_2O)_n$, $n = 1-3$, $CrO_2^+\cdot(N_2O)_m$, $m = 0-2$
				$Cr^+\cdot N_2O$	2	$Cr^+\cdot(N_2O)_2$
Mn^+	$<10^{-13}$	8.6×10^{-10}	$<10^{-4}$	$Mn^+\cdot N_2O$	100	
Fe^+	3.7×10^{-11}	8.6×10^{-10}	0.043	FeO^+	100	$FeO^+\cdot(N_2O)_n$, $n = 1-3$
Co^+	2.1×10^{-12}	8.5×10^{-10}	0.0025	CoO^+	50	$CoO^+\cdot(N_2O)_n$, $n = 1-3$
				$Co^+\cdot N_2O$	50	$Co^+\cdot(N_2O)_m$, $m = 2-3$
Ni^+	6.5×10^{-13}	8.5×10^{-10}	0.00076	$Ni^+\cdot N_2O$	100	$Ni^+\cdot(N_2O)_m$, $m = 2-3$
Cu^+	5.7×10^{-13}	8.4×10^{-10}	0.00067	$Cu^+\cdot N_2O$	100	$Cu^+\cdot(N_2O)_2$
Zn^+	2.4×10^{-12}	8.3×10^{-10}	0.0029	$Zn^+\cdot N_2O$	100	
Ga^+	$<10^{-13}$	8.2×10^{-10}	$<10^{-4}$	$Ga^+\cdot N_2O$	100	
Ge^+	3.6×10^{-10}	8.1×10^{-10}	0.44	GeO^+	100	$GeO^+\cdot N_2O$
As^+	6.7×10^{-10}	8.1×10^{-10}	0.83	AsO^+	100	$AsO^+\cdot N_2O$
Se^+	1.8×10^{-12}	8.0×10^{-10}	0.0023	SeO^+	100	
Rb^+	$<10^{-13}$	7.9×10^{-10}	$<10^{-4}$			
Sr^+	6.3×10^{-11}	7.9×10^{-10}	0.080	SrO^+	100	
Y^+	6.4×10^{-10}	7.8×10^{-10}	0.82	YO^+	100	$YO^+\cdot(N_2O)_n$, $n = 1-3$
Zr^+	7.7×10^{-10}	7.8×10^{-10}	0.99	ZrO^+	55	$ZrO^+\cdot(N_2O)_n$, $n = 1-3$, $ZrO_2^+\cdot(N_2O)_m$, $m = 0-3$
				ZrN^+	45	$ZrN^+\cdot N_2O$
Nb^+	6.5×10^{-10}	7.8×10^{-10}	0.83	NbO^+	65	$NbO_2^+\cdot(N_2O)_n$, $n = 0-3$
				NbN^+	35	$NbNO^+\cdot(N_2O)_m$, $m = 0-3$
Mo^+	3.4×10^{-13}	7.7×10^{-10}	0.00044	$Mo^+\cdot N_2O$	100	$Mo^+\cdot(N_2O)_2$
Ru^+	3.3×10^{-13}	7.6×10^{-10}	0.00043	$Ru^+\cdot N_2O$	100	$Ru^+\cdot(N_2O)_2$
Rh^+	4.0×10^{-13}	7.7×10^{-10}	0.00052	$Rh^+\cdot N_2O$	100	$Rh^+\cdot(N_2O)_2$
Pd^+	8.7×10^{-13}	7.6×10^{-10}	0.00011	$Pd^+\cdot N_2O$	100	$Pd^+\cdot(N_2O)_2$
Ag^+	1.2×10^{-13}	7.6×10^{-10}	0.00016	$Ag^+\cdot N_2O$	100	$Ag^+\cdot(N_2O)_2$
Cd^+	$<10^{-13}$	7.5×10^{-10}	$<10^{-4}$	$Cd^+\cdot N_2O$	100	
In^+	$<10^{-13}$	7.5×10^{-10}	$<10^{-4}$	$In^+\cdot N_2O$	100	
Sn^+	1.0×10^{-13}	7.5×10^{-10}	0.00013	$Sn^+\cdot N_2O$	100	
Sb^+	1.7×10^{-13}	7.5×10^{-10}	0.00023	$Sb^+\cdot N_2O$	100	
Te^+	$<10^{-13}$	7.4×10^{-10}	$<10^{-4}$			
Cs^+	$<10^{-13}$	7.4×10^{-10}	$<10^{-4}$			
Ba^+	2.4×10^{-10}	7.4×10^{-10}	0.32	BaO^+	100	$BaO^+\cdot N_2O$
La^+	5.6×10^{-10}	7.4×10^{-10}	0.76	LaO^+	96	$LaO^+\cdot N_2O$
				LaN^+	4	
Hf^+	6.3×10^{-10}	7.2×10^{-10}	0.88	HfO^+	100	$HfO_2^+\cdot(N_2O)_n$, $n = 0-3$
Ta^+	6.1×10^{-10}	7.1×10^{-10}	0.86	TaO^+	60	$TaO_2^+\cdot(N_2O)_n$, $n = 0-3$
				TaN^+	40	$TaNO^+$
W^+	6.0×10^{-10}	7.1×10^{-10}	0.85	WO^+	100	WO_2^+, $WO_3^+\cdot(N_2O)_n$, $n = 0-2$
Re^+	$<10^{-13}$	7.1×10^{-10}	$<10^{-4}$	ReO^+	100	ReO_2^+
Os^+	5.8×10^{-11}	7.1×10^{-10}	0.082	OsO^+	40	OsO_n^+, $n = 2-4$, NO^+
				OsN^+	60	$OsNO_n^+$, $n = 1-3$
						$OsNO_2^+\cdot N_2O$
Ir^+	2.9×10^{-10}	7.1×10^{-10}	0.41	IrO^+	100	IrO_n^+, $n = 2-3$, $IrO_2^+\cdot N_2O$
Pt^+	1.2×10^{-10}	7.1×10^{-10}	0.17	PtO^+	100	PtO_2^+, $PtO_m^+\cdot N_2O$, $m = 1-2$, NO^+
Au^+	1.2×10^{-12}	7.1×10^{-10}	0.0017	$Au^+\cdot N_2O$	100	$Au^+\cdot(N_2O)_2$
Hg^+	$<10^{-13}$	7.1×10^{-10}	$<10^{-4}$	$Hg^+\cdot N_2O$	100	
Tl^+	$<10^{-13}$	7.1×10^{-10}	$<10^{-4}$	$Tl^+\cdot N_2O$	100	
Pb^+	$<10^{-13}$	7.1×10^{-10}	$<10^{-4}$	$Pb^+\cdot N_2O$	100	
Bi^+	$<10^{-13}$	7.1×10^{-10}	$<10^{-4}$	$Bi^+\cdot N_2O$	100	

[a] Products and product distributions are also included along with calculated collision rate coefficients, k_c, (see text), and reaction efficiencies, k/k_c. [b] Measured effective bimolecular rate coefficient for the loss of the metal ion, with an estimated accuracy of ±30%. [c] Calculated capture rate coefficient (see text). [d] PD = product distribution expressed as a percentage. The product distributions are estimated to be within 5% of their stated value.

All of these addition reactions are expected to be termolecular with He buffer-gas atoms acting as the stabilizing third body. Figures 3 provides data that exemplify the occurrence of each of the reactions 3−5 above. The results in Figure 3 for Sc^+ ($m/z = 45$) show some transmission of Ar^+ ($m/z = 40$) through the first quadrupole. N_2O is able to transfer an electron to Ar^+, and this accounts for the appearance of N_2O^+ in the product spectrum in the Sc^+ results.

3.2. Second-Row Atomic Ions. With the exception of the nonreactions of Rb^+ and Te^+ and the N-atom transfer channel observed with Zr^+ and Nb^+, only O-atom transfer and N_2O addition were observed as primary products for the second-row atomic ions. Secondary dioxide formation was observed for the early transition ions $M^+ = Zr^+$ and Nb^+, but not Y^+. Also, secondary oxidation according to reaction 6 was observed with NbN^+:

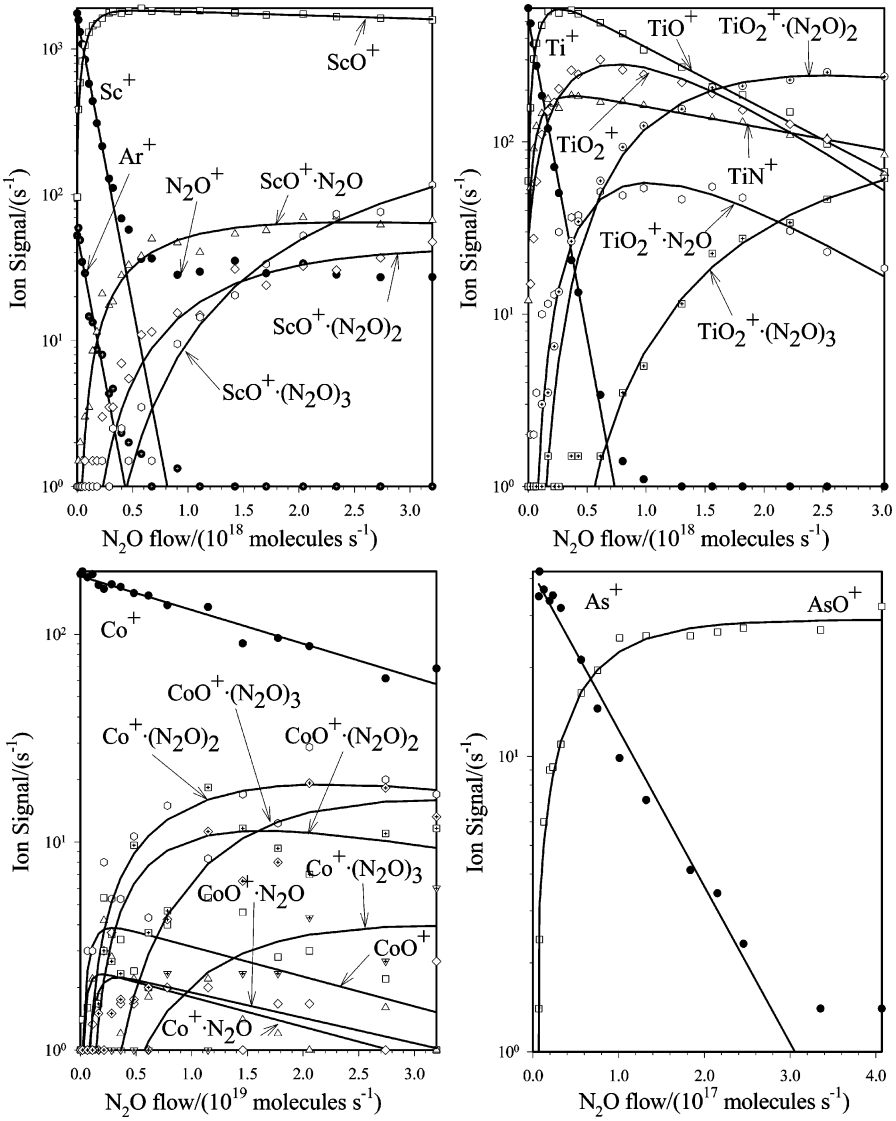

Figure 3. Composite of ICP/SIFT results for the reactions of the early first-row transition-metal ions Sc^+, Ti^+, Co^+, and As^+ with N_2O in helium buffer gas at 0.35 ± 0.01 Torr and 295 ± 2 K.

$$NbN^+ + N_2O \rightarrow (NbNO)^+ + N_2 \qquad (6)$$

Secondary and higher-order N_2O addition was observed for M^+ (all $n = 1$) = Mo^+, Ru^+, Rh^+, Pd^+ and Ag^+, $MO^+ = YO^+$ ($n = 0-2$) and ZrO^+ ($n = 0-2$), ZrN^+ ($n = 0$), $ZrNO^+$ ($n = 0-2$), and $MO_2^+ = ZrO_2^+$ ($n = 0-2$) and NbO_2^+ ($n = 0-2$) cations. Again, all of these addition reactions are expected to be termolecular with He buffer-gas atoms acting as the stabilizing third body and are seen to operate in Figure 4.

3.3. Third-Row Atomic Ions. With the exception of the nonreaction of Cs^+ and the N-atom transfer channel observed with La^+, Ta^+, and Os^+, only O-atom transfer and N_2O addition were observed as primary products for the third-row atomic ions. Figure 5 provides data for the occurrence of competitive O-atom and N-atom transfer in the reactions of La^+, Ta^+, and Os^+. Secondary dioxide formation was observed for the transition ions $M^+ = Hf^+$, Ta^+, W^+, Re^+, Os^+, Ir^+, and Pt^+, but not La^+.

Also, oxidation according to reaction 7 was observed with M = Ta ($n = 0$) and Os (n up to 2):

$$(MNO_n)^+ + N_2O \rightarrow (MNO_{n+1})^+ + N_2 \qquad (7)$$

Higher-order oxidation according to reaction 8 was observed with M = Os (n up to 3) and Ir (n up to 3):

$$MO_n^+ + N_2O \rightarrow MO_{n+1}^+ + N_2 \qquad (8)$$

Secondary and higher-order N_2O addition was observed for $M^+ = Au^+$ ($n = 1$), $MO^+ = BaO^+$ ($n = 0$) and LaO^+ ($n = 0$), $MO_2^+ = HfO_2^+$ ($n = 0-2$), TaO_2^+ ($n = 0-2$), IrO_2^+ ($n = 0$), and PtO_2^+ ($n = 0$) cations. All of these addition reactions are expected to be termolecular with He buffer-gas atoms acting as the stabilizing third body.

3.4. Efficiency of Oxygen-Atom Transfer. O-atom transfer was observed with group 2 atomic ions (Ca^+, Sr^+, Ba^+) and with group 3 (Sc^+, Y^+, La^+), group 4 (Ti^+, Zr^+, Hf^+), and group 5 (V^+, Nb^+, Ta^+) transition-metal ions and with Cr^+, W^+, Re^+, Fe^+, Os^+, Co^+, Ir^+, Pt^+, Ge^+, As^+, and Se^+. Rate coefficients measured for O-atom transfer are in the range of 1.5×10^{-13} cm^3 molecule^{-1} s^{-1} (for Cr^+) to 7.7×10^{-10} cm^3 molecule^{-1} s^{-1} (for Zr^+), but N-atom transfer was observed to compete with O-atom transfer in the reactions with La^+, Ti^+, Zr^+, Nb^+, Ta^+, and Os^+. Only the slow O-atom transfer reactions with Cr^+ and Co^+ (see Figure 3) were observed to compete with N_2O addition.

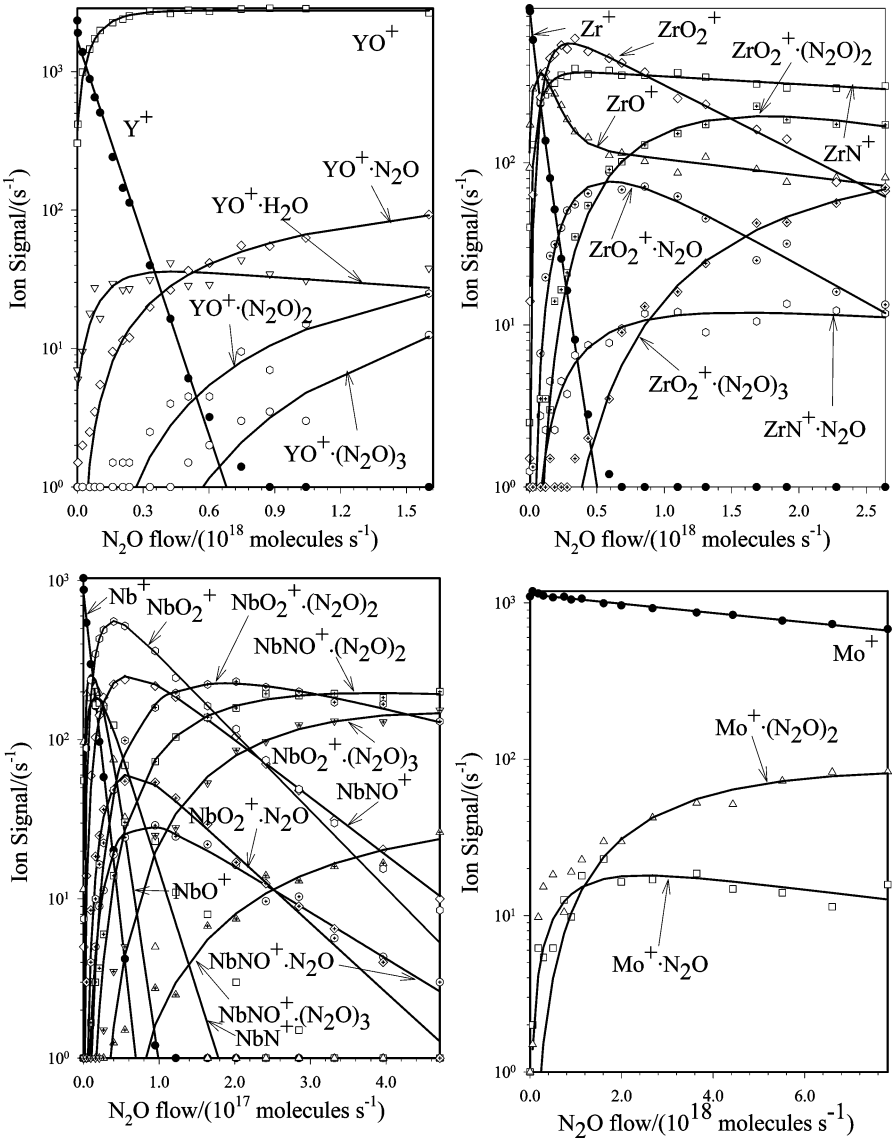

Figure 4. Composite of ICP/SIFT results for the reactions of the early second-row transition-metal ions Y^+, Zr^+, Nb^+, and Mo^+ with N_2O in helium buffer gas at 0.35 ± 0.01 Torr and 295 ± 2 K.

The formation of the monoxide cation by reaction 1a, for which $\Delta H° = OA(N_2) - OA(M^+)$, can be expected to be exothermic for many atomic ions since the O-atom affinity of N_2 to form nitrous oxide is quite low, $OA(N_2) = 40$ kcal mol^{-1}. According to the O-atom affinities listed in Table 3, O-atom transfer is exothermic, and so thermodynamically allowed, for most of the atomic cations investigated. Exceptions are the group 1 ions K^+, Rb^+, and Cs^+ for which O-atom transfer is endothermic and no reactions were observed and the group 8 ion Pd^+, the group 11 ions $Cu^+$and Ag^+, the group 12 ion Zn^+, and the group 13 ion Ga^+ for all of which O-atom transfer is endothermic and slow addition of N_2O was observed.

Figure 6 shows the variation of reaction efficiency with $OA(M^+)$; the reaction efficiency is seen to be high for transition-metal ions with high O-atom affinity, greater than about 120 kcal mol^{-1}, but many other exothermic O-atom transfer reactions proceed with low efficiency.

Fast O-atom transfer from N_2O to Sc^+, Ti^+, and V^+ has been observed previously in 1994 by Ryan et al. using FT-ICR techniques.[38] The unusually low efficiencies of exothermic O-atom transfer to Cr^+, Mn^+, Fe^+, Co^+, and Ni^+ were discovered as early as 1982 by Armentrout, Halle, and Beauchamp in translational energy threshold measurements with an ion-beam apparatus.[39] There is good agreement with our ICP/SIFT measurements: Fe^+, the most reactive ion in the ion-beam experiments, was observed to react with an efficiency of about 0.1 at the lowest energy of these experiments compared to our value of 0.043, and Co^+ with an efficiency about 10 times smaller than that of the Fe^+ reaction compared to our value of 0.0025.

3.4.1. Slow Exothermic but Spin-Forbidden O-Atom Transfer Reactions. Many of the exothermic O-atom transfer reactions have been observed to be very inefficient, less efficient than 1% ($k/k_c < 0.01$): the first-row atomic ions Cr^+, Mn^+, Co^+, Ni^+, and Se^+, the second-row atomic ions Mo^+, Ru^+, Rh^+, Sn^+, and Te^+ ($OA(Cd^+)$ and $OA(In^+)$ are not known), and the third-row atomic ions Re^+, Pb^+, and Bi^+ ($OA(Au^+)$, Hg^+, and Tl^+) are not known).

The failure of the quite exothermic ground-state O-atom transfer reaction with $Mo^+(X^6S)$, reaction 9, to proceed measurably at room temperature has been rationalized previously by Kretschmar et al.[40] in terms of a kinetic barrier arising from a curve crossing that is required for the change in spin multiplicity that is necessary for the overall spin to be conserved. Their FT-ICR study provided an upper limit of 6×10^{-13} cm^3 molecule^{-1} s^{-1} for this reaction which is in good agreement with our result

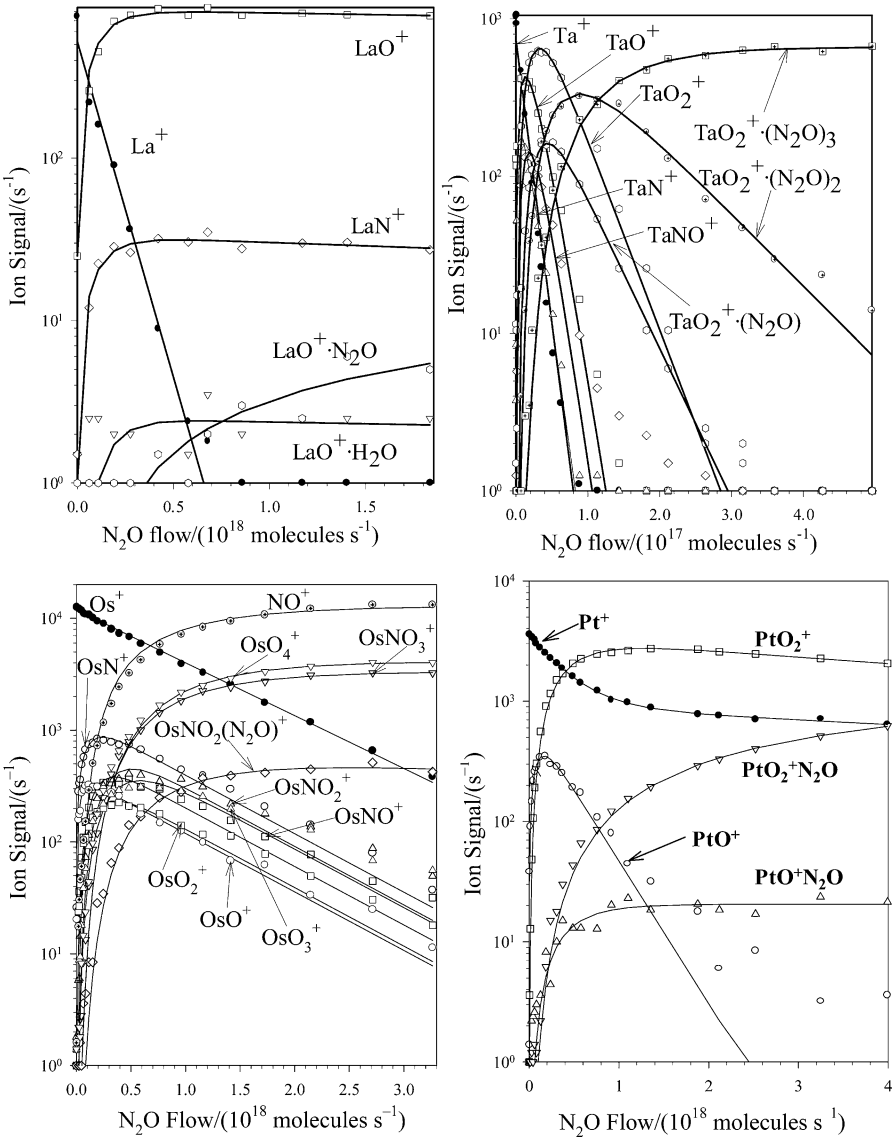

Figure 5. Composite of ICP/SIFT results for the reactions of the early third-row transition-metal ions La^+, Ta^+, Os^+, and Pt^+ with N_2O in helium buffer gas at 0.35 ± 0.01 Torr and 295 ± 2 K. Not shown in the Ta^+ graph are the adduct ions $TaNO^+\cdot(N_2O)_n$ with $n = 1-3$ which were observed to be formed in a manner similar to the N_2O adduct ions observed for TaO_2^+.

that indicates adduct formation with $k = 3.4 \times 10^{-13}$ cm^3 molecule^{-1} s^{-1} ($k/k_c = 0.000\,44$) and an upper limit for O-atom transfer with the same value. Adduct formation was not observed at the much lower pressures of the FT-ICR measurements.

$$Mo^+(X^6S) + N_2O \rightarrow MoO^+(X^4\Sigma^-) + N_2 \qquad \Delta_r H = -77 \text{ kcal mol}^{-1} \quad (9)$$

Spin conservation may also be the deciding factor in many of the other *exothermic* O-atom transfer reactions that were observed to be slow. For spin to be conserved in such reactions for the formation of ground-state products the spins of M^+ and MO^+ must be the same according to the Wigner−Witmer spin conservation rules since the ground states of N_2O and N_2 are both singlets.[41] Electronic ground-state configurations made available in a recent theoretical study by Kretschmar[40b] for first- and second-row transition-metal oxide cations and by others for other atomic oxide cations (see Table 6) indicate that the following exothermic ground-state O-atom transfer reactions, in addition to that of Mo^+, are also spin forbidden (also given are the measured rate coefficients in cm^3 molecule^{-1} s^{-1} and the reaction exothermicities in kcal mol^{-1}):

$$Cr^+(X^6S) + N_2O \rightarrow CrO^+(X^4\Sigma^-) + N_2 \qquad 1.5 \times 10^{-13} \quad -46 \quad (10)$$

$$Mn^+(X^7S) + N_2O \rightarrow MnO^+(X^5\Pi) + N_2 \qquad <10^{-13} \quad -28 \quad (11)$$

$$Co^+(X^3F) + N_2O \rightarrow CoO^+(X^5\Delta) + N_2 \qquad 1.05 \times 10^{-12} \quad -35 \quad (12)$$

$$Ni^+(X^2D) + N_2O \rightarrow NiO^+(X^4\Sigma^-) + N_2 \qquad <6.5 \times 10^{-13} \quad -33 \quad (13)$$

$$Ru^+(X^4F) + N_2O \rightarrow RuO^+(X^6\Sigma^+) + N_2 \qquad <5.7 \times 10^{-13} \quad -48 \quad (14)$$

Armentrout et al.[39] previously have pointed out that the O-atom transfer reactions of $Cr^+(X^6S)$ and $Mn^+(X^7S)$ with N_2O are spin forbidden to form the ground-state metal oxide cations based on the ground-state configurations $CrO^+(X^4\Pi)$ and $MnO^+(X^5\Sigma^+)$. The reaction of $Co^+(X^3F)$ was deemed to be spin allowed by these authors on the basis of the electronic-state

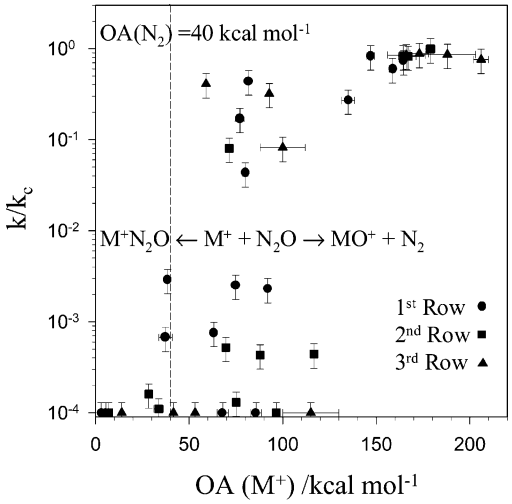

Figure 6. Dependence of the reaction efficiency, k/k_c, on the O-atom affinity, OA, of the cation; k represents the measured reaction rate coefficient for loss of M^+, and k_c is the calculated collision rate coefficient (see Table 5). Some of the reactions include an N-atom transfer channel (see text). Reactions on the right of the dashed line are exothermic for O-atom transfer while those on the left are endothermic.

TABLE 6: Known Electronic-State Configurations for the Ground States of First-, Second-, and Third-Row Atomic Oxide Cations[a]

first row		second row		third row	
ScO^+	$^1\Sigma^+$	YO^+	$^1\Sigma^+$	LaO^+ [c]	$^1\Sigma^+$
TiO^+	$^2\Delta$	ZrO^+	$^2\Sigma$	HfO^+ [d]	$^2\Sigma^+$
VO^+	$^3\Sigma$	NbO^+	$^3\Sigma$	TaO^+ [e]	$^3\Delta$
CrO^+	$^4\Sigma$	MoO^+	$^4\Sigma$		
MnO^+	$^5\Pi$				
FeO^+	$^6\Sigma^+$	RuO^+	$^6\Sigma^+$		
CoO^+	$^5\Delta$	RhO^+	$^3\Sigma$		
NiO^+	$^4\Sigma$	PdO^+	$^4\Sigma$	PtO^+ [f]	$^4\Sigma$
CuO^+	$^3\Sigma$	AgO^+	$^3\Sigma$		
ZnO^+	$^2\Pi$				
AsO^+ [b]	$^1\Sigma$				
SeO^+ [b]	$^2\Pi$				

[a] Taken from ref 40b unless indicated otherwise. [b] Reference 27. [c] Reference 42. [d] Reference 43. [e] Reference 44. [f] Reference 45.

assignment of $^3\Sigma$ rather than $^5\Delta$ for the ground state of CoO^+ (although these authors also reported a low efficiency for the reaction of $Co^+(X^3F)$). The rate coefficient for the O-atom transfer reaction with Co^+, $k = 1.05 \times 10^{-12}$ cm^3 molecule^{-1} s^{-1}, is in fact somewhat anomalous in that it is about 1 order of magnitude higher than those measured for the remaining spin-forbidden reactions. So if the $^3\Sigma$ state of CoO^+ is only marginally higher in energy than the ground-state reaction exothermicity of about 35 kcal mol^{-1}, a slow slightly endothermic, but spin-allowed, reaction becomes possible.

3.4.2. Fast Exothermic but Spin-Forbidden O-Atom Transfer Reactions. Other exothermic O-atom transfer reactions have been observed to be very efficient, $k/k_c \geq 0.60$, but spin forbidden for formation of the ground state products. Some of these, for which the ground-state configuration of the product atomic oxide is known, are shown in Table 7. All of these reactions are highly exothermic, by more than 118 kcal mol^{-1}, for formation of ground-state products. The high efficiency of these spin-forbidden reactions can be rationalized in terms of the formation of exited ionic and/or excited neutral products that is both exothermic and spin allowed. We can rule out significant contributions of ions that are populated at 5500 K in spin states other than the ground state and that are not quenched by radiation or collision before reaching the reaction region. The populations of such ions are too low judging from the linearity of the measured semilogarithmic decays of the reacting atomic ions and from their initial populations at 5500 K.

TABLE 7: Fast Exothermic O-Atom Transfer Reactions That Are Spin Forbidden for Formation of Ground State Oxide Cations

M^+	M^+ term[a]	MO^+ term	$\Delta H°$ (kcal mol^{-1})	rate coefficient[b] (cm^3 molecule^{-1} s^{-1})
Ti^+	X^4F (85%)	$X^2\Delta$	-118.6 ± 1.6	5.3×10^{-10} (0.60)
As^+	X^3P	$X^1\Sigma$	-107	6.7×10^{-10} (0.83)
Zr^+	X^4F (64%)	$X^2\Delta$	-139.0 ± 2.5	7.7×10^{-10} (0.99)
Nb^+	X^5D (79%)	$X^3\Sigma$	-124.4 ± 2.5	6.5×10^{-10} (0.83)
La^+	X^3F (80%)	$X^1\Sigma$	-166 ± 4	5.6×10^{-10} (0.76)
Ta^+	X^5F (62%)	$X^3\Sigma$	-148 ± 5	6.1×10^{-10} (0.86)

[a] The population of atomic ions with the same spin state as the ground-state including the ground state (given in Table 1) is given in parentheses. [b] The efficiency of reaction, k/k_c (see text), is given in parentheses.

Very exothermic O-atom transfer reactions with N_2O can lead to the formation of an electronically excited atomic oxide cation and/or electronically excited N_2. Formation of the latter, which requires 143 kcal mol^{-1} to form $N_2(A^3\Sigma)$, is spin allowed and exothermic for reactions 15 and 16 by 23 ± 4 and 5 ± 5 kcal mol^{-1}, respectively.

$$La^+ (X^3F) + N_2O(X^1\Sigma) \rightarrow LaO^+ (X^1\Sigma) + N_2(A^3\Sigma) \quad (15)$$

$$Ta^+ (X^5F) + N_2O(X^1\Sigma) \rightarrow TaO^+ (X^3\Delta) + N_2(A^3\Sigma) \quad (16)$$

The reaction with Zr^+, reaction 17, is spin allowed and endothermic by only 4 ± 3 kcal mol^{-1}.

$$Zr^+ (X^4F) + N_2O(X^1\Sigma) \rightarrow ZrO^+ (X^2\Delta) + N_2(A^3\Sigma) \quad (17)$$

Other pathways are likely to exist for these, and other reactions that are more endothermic for the formation of excited-state $N_2(A^3\Sigma)$, that involve formation of low-lying excited states of the monoxide cations. For example, the triplet state, LaO^+, makes reaction 18 spin allowed

$$La^+ (X^3F) + N_2O(X^1\Sigma) \rightarrow LaO^+ (^3\Delta) + N_2(X^1\Sigma) \quad (18)$$

and the quartet state, TiO^+ ($^4\Delta$), makes reaction 19 spin allowed.

$$Ti^+ (X^4F) + N_2O (X^1\Sigma) \rightarrow TiO^+ (^4\Delta) + N_2(X^1\Sigma) \quad (19)$$

Unfortunately, the exothermicities of reactions 18 and 19 cannot be assessed; not enough is known about the energies of the excited oxide states. Recent calculations by Petrie[27] indicate that the reaction of $As^+(X^3P)$ can form an excited triplet state of AsO^+ that is exothermic by 1.6 kcal mol^{-1} (formation of the ground-state AsO^+ ($^1\Sigma$) is spin forbidden). We are not aware of required electronic-state information for the oxide cations in Table 7 but suggest that exothermic spin-allowed routes to form excited atomic oxide cations are also available for the reactions of V^+ (^5D), Zr^+ (X^4F), Nb^+ (X^5D), and Ta^+ (X^5F) with N_2O. It is interesting to note that the earlier ICR experiments of Kappes and Staley found that VO^+ produced from V^+ and N_2O reacts with H_2 and CH_4 to produce VOH^+ while VO^+ produced by the much less exothermic reaction of V^+ with O_2 does not.[6] Similar results were obtained with TiO^+. This behavior is consistent with our suggestion that the reactions of Ti^+ and V^+ form excited electronic states of the atomic oxide cations upon

their formation from N_2O (but not when formed from O_2). We can also note that these excited electronic states would then likely lie below 79 kcal mol^{-1} (OA(O) − OA(N_2).

3.4.3. Fast and Slow Exothermic and Spin-Allowed O-Atom Transfer Reactions. A spin-allowed reaction with N_2O involving ground-state reactants and products requires that the spin quantum numbers $s(X^+) = s(XO^+)$. This turns out to be very much the exception rather than the rule for the 33 exothermic reactions investigated here.

Available information on the electronic configurations of ground-state atomic oxide cations indicates that only the reactions of Fe^+, Zn^+, Y^+, Rh^+, and Hf^+ with N_2O, reactions 20−24, are spin allowed.

$$Fe^+ (X^6D) + N_2O(X^1\Sigma) \rightarrow FeO^+ (X^6\Sigma) + N_2(X^1\Sigma)$$
$$3.7 \times 10^{-11} \quad -40 \quad (20)$$

$$Zn^+ (X^2S) + N_2O(X^1\Sigma) \rightarrow ZnO^+ (X^2\Pi) + N_2(X^1\Sigma)$$
$$<2.4 \times 10^{-12} \quad +1.5 \pm 1.2 \quad (21)$$

$$Y^+ (X^1S) + N_2O(X^1\Sigma) \rightarrow YO^+ (X^1\Sigma) + N_2(X^1\Sigma)$$
$$6.4 \times 10^{-10} \quad -127 \quad (22)$$

$$Rh^+ (X^3F) + N_2O(X^1\Sigma) \rightarrow RhO^+ (X^3\Sigma) + N_2(X^1\Sigma)$$
$$<4.0 \times 10^{-13} \quad -30 \quad (23)$$

$$Hf^+ (X^2D) + N_2O(X^1\Sigma) \rightarrow HfO^+ (X^2\Sigma) + N_2(X^1\Sigma)$$
$$6.4 \times 10^{-10} \quad -133 \quad (24)$$

Only two of these reactions, those with Y^+ (X^1S) and Hf^+ (X^2D), are fast, $k > 6 \times 10^{-10}$ cm^3 molecule^{-1} s^{-1}. These are also the two that are by far the most exothermic. The O-atom transfer reaction with Fe^+ (X^6D) is somewhat slower and only moderately exothermic. The O-atom transfer reaction with Zn^+ (X^2S) is slightly endothermic and very slow, $k < 2.4 \times 10^{-12}$ cm^3 molecule^{-1} s^{-1}. Only the O-atom transfer reaction with Rh^+ (X^3F) appears not to be consistent in that it apparently is spin allowed and moderately exothermic but extremely slow. It is noteworthy however that, of the reactions that are exothermic, it is the least exothermic. This prompted us to look into the possible presence of a kinetic barrier associated with the breaking of the O−N_2 bond and arising from the formation of the transition state along the reaction coordinate.

We have performed a density functional theory (DFT) study of the reaction pathway $M^+ + N_2O \rightarrow MO^+ + N_2$ for $M^+ = Rh^+$ (very slow reaction), Fe^+ (slow), and Y^+ (very fast). All predictions were made using the Gaussian 98 program suit[46] with hybrid B3LYP[47] exchange-correlation functional. The 6-311+G(d) triply split basis set[48] augmented with diffuse and polarization functions was used for the light atoms. The Stuttgart/Dresden relativistic ECP[49] and Dunning basis set[50] were employed for the metal atoms. The connection between critical points on the potential-energy surface was verified using the IRC procedure as implemented in Gaussian 98. All energies reported include zero-point vibrational energy corrections. The potential-energy profiles for oxygen transfer along with structures are shown in Figure 7. Metal ions form the prereaction complex $[M\cdots ON_2]^+$, the oxygen transfer proceeds through a barrier and results in a postreaction complex $[MO\cdots N_2]^+$ that dissociates into MO^+ and N_2. The origin of the barrier to oxygen-atom transfer has been explored previously and attributed to the fact that the ground state of N_2O ($^1\Sigma^+$) does not correlate with the ground state of N_2 ($^1\Sigma_g$) + O (^{3}P).[39] Formally

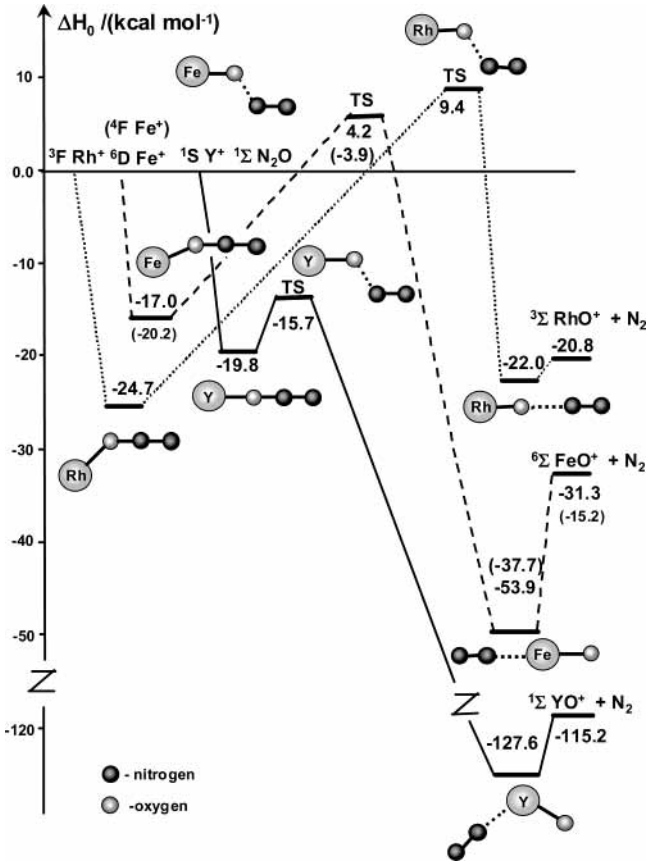

Figure 7. Potential-energy profiles for the reaction $M^+ + N_2O \rightarrow MO^+ + N_2$ ($M^+ = Rh^+$, Fe^+, Y^+) predicted with the B3LYP/sdd/6-311+G(d) method. Relative enthalpies are inserted for the low-spin reaction pathway for Fe^+.

the reaction of Fe^+ with N_2O can involve both the high-spin and low-spin states typical of Fe^+ and a double-crossing of quartet and sextet surfaces.[51,52] The quartet surface provides a lower-energy path. However, the ^{6}D−^{4}F mixing at the first crossing is extremely inefficient[51c,52b,c] so that the reaction of Fe^+ (^{6}D) with N_2O proceeds only on the sextet surface. The binding energies for prereaction complexes are −24.7, −17.0, and −19.8 kcal mol $^{-1}$ for Rh^+ (^{3}F), Fe^+ (^{6}D), and Y^+ (^{1}S), respectively. The reaction barriers to oxygen transfer to Rh^+ (^{3}F) and Fe^+ (^{6}D) are predicted to be 9.6 and 4.2 kcal mol^{-1} *above* the dissociation limit to $M^+ + N_2O$, and these are consistent with the very slow and slow reactions observed with Rh^+ and Fe^+, respectively ($k < 4.0 \times 10^{-13}$ and 3.7×10^{-11} cm^3 molecule^{-1} s^{-1}, respectively). In contrast, for the strongly exothermic oxygen transfer to Y^+, the reaction barrier is predicted to be 15.7 kcal mol $^{-1}$ *below* the dissociation limit, and this is in accord with the experimental observation of a very fast reaction with Y^+ ($k = 6.4 \times 10^{-10}$ cm^3 molecule^{-1} s^{-1}). Thus, for these three reactions, theory predicts that the barrier to oxygen transfer increases as the exothermicity of reaction decreases and that it becomes the deciding factor in determining the rate of these spin-allowed exothermic reactions.

3.4.4. Breakdown of Spin Control. A number of the reactions involving third-row transition-metal cations were observed to be fast despite being spin forbidden for formation of ground-state products and probably not sufficiently exothermic to form spin-allowed electronically exited products (the highly exothermic reaction 27 may be a poor example, but it cannot be properly evaluated without knowledge of the electronic configuration and energies of the excited states of WO^+; formation of $N_2(A^3\Sigma)$ is not exothermic):

$$Ir^+ (X^5F) + N_2O(X^1\Sigma) \rightarrow IrO^+ (X^3\Sigma) + N_2(X^1\Sigma) \quad 2.9 \times 10^{-10} \quad -19 \quad (25)$$

$$Pt^+ (X^2D) + N_2O(X^1\Sigma) \rightarrow PtO^+ (X^4\Sigma) + N_2(X^1\Sigma) \quad 1.2 \times 10^{-10} \quad -37 \quad (26)$$

$$W^+ (X^6D) + N_2O(X^1\Sigma) \rightarrow WO^+ (X^4\Sigma) + N_2(X^1\Sigma) \quad 6.0 \times 10^{-10} \quad -126 \quad (27)$$

For these reactions we suggest that spin mixing occurs in the formation of the transition-metal oxide cation so that spin control breaks down: the low-lying electronic states of Ir^+, Pt^+, and W^+ are ^3F, ^4F, and ^4F, respectively. The importance of spin−orbit coupling in platinum-containing species including PtO^+ has been addressed theoretically by Heinemann et al.[45] The reaction with Re^+ (X^7S), reaction 28

$$Re^+ (X^7S) + N_2O(X^1\Sigma) \rightarrow ReO^+ (X^5\Sigma) + N_2(X^1\Sigma) \quad <10^{-13} \quad -75 \quad (28)$$

apparently is an exception, but in this case spin mixing is likely to be unfavorable because of the 1.7 eV gap between the ground state and the first excited ^5D state of Re^+. Spin conservation in the reaction with Os^+ cannot be assessed because of the unknown electronic configuration of the ground electronic state of Os^+.

The measured decay for the reaction of Pt^+ with N_2O showed a second slow component (see Figure 5) with $k = 4.0 \times 10^{-12}$ cm^3 molecule^{-1} s^{-1}. Extrapolation back to zero flow indicates a 25% contribution of the slow component to the initial Pt^+ population. This number, probably not fortuitously, is roughly equal to our calculated excited-state percentage at 5500 K (36.3%). So it seems that most of the excited $Pt^+(^4F,6s^1,5d^8)$ ions are not deactivated under our experimental operating conditions and react slowly with N_2O. This is the only case of this kind that we have knowingly encountered. The low rate coefficient is surprising since O-atom transfer would be spin allowed and exothermic by (37 kcal mol^{-1} + the ^4F excitation energy).

3.5. Nitrogen-Atom Transfer. Table 5 shows that nitrogen-atom transfer was observed to compete in the reactions of N_2O with La^+ (4%, 2%[7]), Ti^+ (22%), Zr^+ (45%), Nb^+ (35%), and Ta^+ (40%), and we have reported separately the observation of N-atom transfer with Ce^+ (25%) in our study of the reactions of lanthanide cations with N_2O.[4] The interesting competition of O-atom and N-atom transfer in the reactions of Zr^+ and Nb^+ with N_2O can be seen in Figure 3 while that for the reactions of La^+ and Ta^+ can be seen in Figure 4.

The N-atom affinity of NO to form nitrous oxide is understandably quite large, NA(NO) = 114.9 ± 0.1 kcal mol^{-1},[1] and this means that the N-atom transfer reaction 1b is likely to be endothermic at room temperature. The known metal ion N-atom affinities listed in Table 2, of which there are only a few, are not well established. However N-atom transfer is likely to be endothermic with Sc^+ (NA = 63.1 kcal mol^{-1}), Cr^+ (NA = 49.5 kcal mol^{-1}), and Hf^+ (NA = 69 ± >12), and probably also V^+ (NA = 89 ± 42 or 87.1 kcal mol^{-1}), and we did not observe N-atom transfer with these ions. The numbers in Table 2 also indicate that N-atom transfer is possibly exothermic with Nb^+ (NA = 134 kcal mol^{-1}) and Ti^+ (NA = 143 ± 62 or 97.8 kcal mol^{-1}), and we have observed this transfer with both of these ions, 35% and 22%, respectively.

As far as we are aware, there have been only two previous observations of N-atom transfer from N_2O to atomic cations. The uranium cation, U^+, has been observed by Heinemann and Schwarz to react with N_2O, $k = 8.5 \times 10^{-10}$ cm^3 molecule^{-1} s^{-1}, in an FT-ICR mass spectrometer and to abstract N in 30% of its collisions with N_2O.[53] These authors also determined NA(U^+) to be 120 ± 10 kcal mol^{-1} from bracketing experiments. Rodgers et al.[54] have reported the appearance of CuN^+ in the reaction of $Cu^+(^1S)$ with N_2O at very high translational energies (above 14 eV, CM).

3.6. N_2O Addition Reactions. Addition of N_2O was observed exclusively with the first-row cations Mn^+, Ni^+, Cu^+, Zn^+, and Ga^+, the second-row cations Mo^+, Ru^+, Rh^+, Pd^+, Ag^+, Cd^+, In^+, Sn^+, and Sb^+, and the third-row cations Au^+, Hg^+, Tl^+, Pb^+, and Bi^+. All these addition reactions are presumed to occur by the collisional stabilization reaction 29 at 0.35 Torr of He

$$M^+ + N_2O + He \rightarrow M^+N_2O + He \quad (29)$$

rather than by radiative association (however, pressure dependent studies were not performed). They were observed to proceed with relatively small effective bimolecular rate coefficients, $\leq 2.4 \times 10^{-12}$ cm^3 molecule^{-1} s^{-1}. A possible reason for the low efficiency of addition is a low binding energy of the adduct ion: the electrostatic interaction between the atomic ions and N_2O is relatively weak because of the low dipole moment of N_2O (0.167 D).[37c] Extensive literature search yields very little information on binding energies of bare ions and N_2O molecules. No reactions or products were observed with K^+, Rb^+, and Cs^+ (group 1) which have a rare-gas electron configuration and with Te^+ that has a p^3 half-filled electron configuration. Failure to observe N_2O addition with the last four ions can be attributed to the weaker bonding with N_2O expected from these electronic configurations. Weak bonding will decrease the rate of addition and may also lead to adduct dissociation upon sampling.

Two N_2O molecules were observed to add sequentially to the first-row cations Ni^+ and Cu^+, the second-row cations Mo^+, Ru^+, Rh^+, Pd^+, and Ag^+, and the third-row cation Au^+. Only Ni^+ was observed to add three N_2O molecules in the N_2O flow range investigated. The secondary rate coefficients for addition were always higher than the primary ones, $k > 5 \times 10^{-12}$ cm^3 molecule^{-1} s^{-1}, and this can be attributed to the increased number of degrees of freedom in the secondary reaction intermediate which leads to longer lifetimes and so higher rates of collisional stabilization. Resonant photodissociation spectroscopy of gaseous Ni^+N_2O has provided a ground-state binding energy of 1.096 ± 0.003 eV[55], and the adduct ion has been predicted to have a linear structure.[56] It is interesting to note that this binding energy is comparable to those calculated here for some other N_2O adducts and illustrated in Figure 7.

N_2O addition was also observed with many of the metal oxide ions that were formed with the early transition-metal ions (see Table 5). For these ions, except SeO^+, higher-order chemistry was observed involving multistep addition of N_2O to their monoxides or dioxides. Typically, monoxide and dioxide cations accept up to three N_2O molecules with few exceptions.

3.7. Oxidation of MN^+. The MN^+ produced by N-atom transfer generally did not exhibit any higher-order bimolecular reactions. For example, MN_2^+ ions were not produced in secondary reactions of MN^+ with N_2O. However, fast secondary reactions of type 30, leading

$$MN^+ + N_2O \rightarrow (MNO)^+ + N_2 \quad (30)$$

TABLE 8: Measured Rate Coefficients (k in Units of cm^3 molecule^{-1} s^{-1}) and Available Thermodynamics (in Units of kcal mol^{-1}) for the Formation of MO_2^+ from the Reaction of MO^+ with N_2O

M^+	k	$D(O-MO^+)$[a]	$\Delta H°$
Ti^+	6.4×10^{-11}	81	−37
V^+	5.2×10^{-11}	90	−46
Cr^+	8.4×10^{-13}	66	−22
Zr^+	6.9×10^{-10}	89	−45
Nb^+	4.8×10^{-10}	132	−88
Hf^+	4.9×10^{-10}		
Ta^+	4.4×10^{-10}	140	−96
W^+	1.0×10^{-10}	132	−88
Re^+	3.0×10^{-13}	65	−21
Os^+	1.35×10^{-9}	105	−61
Ir^+	5.4×10^{-10}	125	−81
Pt^+	5.5×10^{-10}	75	−31

[a] Values taken from ref 18.

to the oxidation of MN^+, were observed with NbN^+ ($k = 2.4 \times 10^{-10}$ cm^3 molecule^{-1} s^{-1}), TaN^+ ($k = 1.4 \times 10^{-9}$ cm^3 molecule^{-1} s^{-1}), and OsN^+ ($k = 5.3 \times 10^{-10}$ cm^3 molecule^{-1} s^{-1}) to form $(NbNO)^+$, $(TaNO)^+$, and $(OsNO)^+$, respectively. The structures of the observed $(MNO)^+$ ions, whether OMN^+, MON^+, or MNO^+, are not known, and these ions appear not to have been observed previously by others.

Higher-order oxidation was observed with $OsNO^+$ according to reactions 31 and 32 with product distributions of 40% (31a) and 60% (31b) and of 85% (32a) and 15% (32b).

$$(OsNO)^+ + N_2O \rightarrow (OsNO_2)^+ + N_2 \quad (31a)$$

$$\rightarrow NO^+ + OsN_2O \quad (31b)$$

$$(OsNO_2)^+ + N_2O \rightarrow (OsNO_3)^+ + N_2 \quad (32a)$$

$$\rightarrow (OsNO_2)^+(N_2O) \quad (32b)$$

Reaction 31 is particularly interesting since the two bimolecular channels 31a and 31b are isoelectronic.

3.8. Dioxide and Higher Oxide Formation from MO^+. A second O-atom transfer, reaction 2, was observed with the group 4, 5, and 6 transition-metal ions (except Mo^+) as well as the third-row ions Re^+, Os^+, Ir^+, and Pt^+. The atomic ions W^+, Os^+, and Ir^+ formed trioxides in sequential O-atom transfer reactions, and even the tetroxide OsO_4^+ was observed to be formed by sequential O-atom transfer to Os^+ (see Figure 5).

The kinetics and thermochemistry of the second-order O-atom transfer reactions leading to formation of MO_2^+ are given in Table 8. As in the formation of monoxides, the second step of O-atom transfer tends also to be very fast, except for the formation of ReO_2^+ of which only traces were observed.

The reaction of Pt^+ with N_2O has been investigated very recently at the lower pressures of an FT-ICR mass spectrometer.[51] Sequential O-atom transfer was observed to form PtO_2^+ with rate coefficients of 0.7×10^{-10} and 1.9×10^{-10} cm^3 molecule^{-1} s^{-1} for the addition of the first and second O-atom, respectively. Our values of 1.2×10^{-10} and 5.5×10^{-10} cm^3 molecule^{-1} s^{-1} are somewhat higher, as is the ratio of rate coefficients that is 4.6 compared to 2.7. The reactivity studies and computations that were also reported by Brönstrup et al.[57] are in keeping with the dioxide structure $OPtO^+$ for PtO_2^+ produced by the sequential O-atom transfer.

MO_3^+ formation by reaction 33 was observed with W^+, Os^+, and Ir^+ with rate coefficients of 1.9×10^{-10}, 3.8×10^{-10}, and 5.4×10^{-10} cm^3 molecule^{-1} s^{-1}, respectively.

SCHEME 1

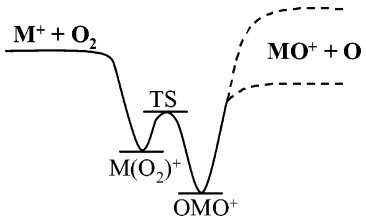

$$MO_2^+ + N_2O \rightarrow MO_3^+ + N_2 \quad (33)$$

To the best of our knowledge, the formation of IrO_3^+ ion has never been observed before.

Os^+ was observed to react sequentially with N_2O ultimately to produce OsO_4^+ with rate coefficients of $k = 0.58$, 13.5, 3.8, and 3.1×10^{-10} cm^3 molecule^{-1} s^{-1}, respectively (see Figure 5). The sequential oxidation of Os^+ to OsO_4^+ has been reported previously using OsO_4 as the oxidant and a FT-ICR mass spectrometer.[58] The following O-atom affinities were also reported: $D(Os^+-O) = 99.91 \pm 12.1$ kcal mol^{-1}, $D(OsO^+-O) = 105.3 \pm 12.1$ kcal mol^{-1}, $D(OsO_2^+-O) = 105.3 \pm 12.1$ kcal mol^{-1}, and $D(OsO_3^+-O) = 71.4 \pm 12.1$ kcal mol^{-1}. These O-atom affinities indicate clearly that each of the four steps leading to the formation of OsO_4^+ in N_2O is exothermic.

3.9. Structures of Oxides. A number of isomers are possible for the higher oxides MO_n^+ with $n \geq 2$. For example, three isomers exist for $n = 2$: an end-on metal dioxygen complex, a side-on complex, and an inserted metal dioxide.[18] For trioxides and tetroxides the number of isomers will be correspondingly higher. This means that it becomes complicated to predict which isomer may be preferred in the formation of the higher oxide cations. Some insight into the bond strengths and connectivities of metal oxide cations has been provided by theory. For example, Schröder et al.[59] have reported the calculated potential-energy surfaces for $[Fe,O_2]^+$ and $[Cr,O_2]^+$ and Brönstrup et al.[57] the surface for $[Pt,O_2]^+$. Both the dioxygen and the inserted metal dioxide cation structures were included, together with an assessment of the barrier for isomerization in the case of $[Fe,O_2]^+$ and $[Cr,O_2]^+$. The barrier is small (5 kcal mol^{-1}) for the spin- and symmetry-allowed isomerization in $[Fe,O_2]^+$ and large for the spin-forbidden isomerization in $[Cr,O_2]^+$. The inserted metal dioxide cation was found to be the global minimum on all three $[M,O_2]^+$ surfaces. A generic potential-energy surface for $[M,O_2]^+$ is shown in Scheme 1.

In this study we have performed multicollision CID experiments[60] to explore the bonding in the higher oxide cations: ions are accelerated by an auxiliary electrostatic field in the ion-sampling region so that multiple collisions with buffer-gas atoms produce dissociation. Collisions with buffer-gas He atoms were found not to promote metal−oxygen bond cleavage in the available range in nose-cone voltage up to −80 V. This is indicative of relatively strong bonding. On the other hand, experiments in Ar buffer which makes available a higher CM energy did show metal−oxygen bond cleavage with many of the higher oxides observed. Thus, the following dioxides: TiO_2^+, ZrO_2^+, HfO_2^+, VO_2^+, NbO_2^+, TaO_2^+, and WO_3^+ were observed to decompose primarily by the consecutive detachment of O-atoms from oxide ions according to reaction 34, while the oxides, CrO_2^+, ReO_2^+, and PtO_2^+ primarily appeared to lose O_2 molecules according to reaction 35 under the same conditions (see Figure 8).

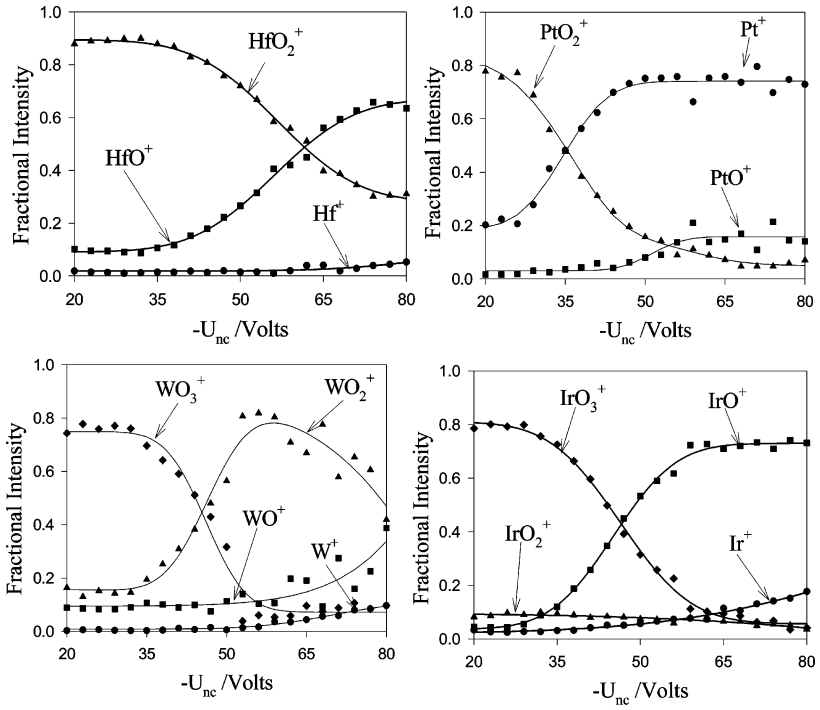

Figure 8. Multicollision-induced dissociation spectra for oxide cations of Hf, Pt, W, and Ir in argon buffer gas. The flows of N_2O are 1.9×10^{17} (Hf), 3.7×10^{18} (Pt), 3.6×10^{17} (W), and 3.4×10^{17} molecules s^{-1} (Ir).

$$MO_2^+ \rightarrow MO^+ \rightarrow M^+$$
$$\text{for M} = Ti^+, Zr^+, Hf^+, V^+, Nb^+, Ta^+, W^+ \quad (34)$$

$$MO_2^+ \rightarrow M^+ + O_2$$
$$\text{for M} = Cr^+, Re^+, Pt^+ \quad (35)$$

A small fraction of the PtO_2^+ also appeared to dissociate by O loss at higher energies.

We can understand these results in terms of the generic potential-energy profile in Scheme 1 if we distinguish between two cases according to whether the $MO^+ + O$ dissociation limit lies above or below the $M^+ + O_2$ dissociation limit. We need not know the global minimum of $[M,O_2]^+$ since multiple collisions are expected to promote isomerization and so dissociation along the lowest energy dissociation channel. (The unfortunate corollary is that we cannot learn about the bond connectivity of the dioxide cations formed in our experiments using multicollision-induced dissociation). The M^+ ions whose dioxides undergo reaction 34 all have $OA(M^+) > OA(O)$ so that the $MO^+ + O$ dissociation limit lies below the $M^+ + O_2$ dissociation limit and loss of O is observed. The M^+ ions whose dioxides undergo reaction 35 all have $OA(M^+) < OA(O)$ so that the $MO^+ + O$ dissociation limit lies above the $M^+ + O_2$ dissociation limit and loss of O_2 is observed. So it appears that the dissociation is thermodynamically controlled. This is true even for the special case of $[Cr,O_2]^+$ since the large barrier for the spin-forbidden isomerization of $OCrO^+$ (^2X) to $Cr(O_2)^+$ (^6X) which lies above the $M^+ + O_2$ dissociation limit is still below the $MO^+ + O$ dissociation limit (the term symbols were not given).[53] A possible exception is PtO_2^+ (formed by the successive oxidation of Pt^+ with N_2O) which has been assigned the dioxide structure $OPtO^+$ by Brönstrup et al on the basis of reactivity studies and on the basis of calculations which indicate that $OPtO^+$ is the global minimum on the $[Pt,O_2]^+$ surface.[57] Our multi-CID results indicate some O loss at higher energies possibly due to sufficient multicollisional activation of the $OPtO^+$ isomer to the $PtO^+ + O$ dissociation limit. This result is completely consistent with the CID result obtained at the much lower pressures of guided-ion-beam tandem mass spectrometer measurements for the dissociation of $OPtO^+$ (formed by sequential reactions of Pt^+ with N_2O) by collisions with Xe reported very recently by Zhang and Armentrout.[61]

Figure 8 also shows the occurrence of the dissociation reactions 36 and 37.

$$WO_3^+ \rightarrow WO_2^+ + O \quad (36)$$

$$IrO_3^+ \rightarrow IrO^+ + O_2 \quad (37)$$

With the assumption that these multicollision-induced dissociations are also thermodynamically controlled, we can derive limits for the bond dissociation energies $D(OW^+-O) > OA(O)$ and $D(OIr^+-O) < OA(O)$, where $OA(O) = 119.1 \pm 0.1$ kcal mol^{-1}.[5]

These compare reasonably well with currently recommended values of 140 and 125 kcal mol^{-1} (uncertainties were not indicated), respectively.[19]

4. Conclusions

The substantial kinetic data obtained in this study clearly demonstrate that atomic cations initiate a very rich chemistry in their reactions with N_2O. In contrast to our previous finding with O_2,[1a] O-atom transfer from N_2O is generally not thermodynamically controlled and exhibits periodic trends in reactivity. An intrinsic reaction barrier is present that can reduce the efficiency of slightly exothermic O-atom transfer. Violation of spin conservation also can substantially reduce reaction efficiency: the potential-energy curve crossing that is required for the change in spin multiplicity that is necessary for the overall spin to be conserved gives rise to a kinetic barrier. Spin conservation in highly exothermic reactions can favor the formation of excited oxide cations or even excited N_2.

N_2O is a source of both O and N atoms for selected atomic cations and so can lead to both cationic oxide and nitride formation. Sequential O-atom transfer can lead to higher oxide

formation with selected atomic cations, particularly with W^+, Os^+, and Ir^+, while metal nitrosyl cation formation occurs in the oxidation of the cationic nitrides of Nb^+ and Ta^+. Results obtained with the multicollision-induced dissociation experiments of dioxide cations indicate that the dissociations are thermodynamically controlled and so do not provide structural information for the dioxides.

Acknowledgment. Continued financial support from the Natural Sciences and Engineering Research Council of Canada is greatly appreciated. Also, we acknowledge support from the National Research Council, the Natural Science and Engineering Research Council, and MDS SCIEX in the form of a Research Partnership Grant. As holder of a Canada Research Chair in Physical Chemistry, Diethard K. Bohme thanks the contributions of the Canada Research Chair Program to this research.

Supporting Information Available: Total energies and Cartesian coordinates of all the reported structures. This material is available free of charge via the Internet at http://pubs.acs.org.

References and Notes

(1) (a) Koyanagi, G. K.; Caraiman, D.; Blagojevoc, V.; Bohme, D. K. *J. Phys. Chem. A* **2002**, *106*, 4581. (b) Caraiman, D.; Bohme, D. K. *J. Phys. Chem. A* **2002**, *106*, 9705. (c) Caraiman, D.; Koyanagi, G. K.; Bohme, D. K. *J. Phys. Chem. A* **2004**, *108*, 978.

(2) (a) Murad, E. *Geophys. Res.* **1978**, *83*, 5525. (b) Ferguson, E. E.; Fehsenfeld, F. C. *Geophys. Res.***1968**, *73*, 6215.

(3) See, for example, Chen, P.; Cabrito, I.; Moura, J. J. G.; Moura, I.; Solomon, E. I. *J. Am. Chem. Soc.* **2002**, *124*, 10497.

(4) Koyanagi, G. K.; Bohme, D. K. *J. Phys. Chem. A* **2001**, *105*, 8964.

(5) Lias, S. G.; Bartmess, J. E.; Liebman, J. F.; Holmes, J. L.; Levin, R. D.; Mallard, W. G. *J. Phys. Chem. Ref. Data* **1988,** *17* (Suppl. 1).

(6) Kappes, M. M.; Staley, R. H. *J. Phys. Chem.* **1981**, *85*, 942.

(7) Schröder, D.; Schwarz, H. *Angew. Chem., Int. Ed. Engl.* **1995**, *34*, 1973.

(8) Kappes, M. M.; Staley, R. H. *J. Am. Chem. Soc.* **1981**, *103*, 1286.

(9) Blagojevic, V.; Jarvis, M. J. Y.; Flaim, E.; Koyanagi, G. K.; Lavrov, V. V.; Bohme, D. K. *Angew. Chem., Int. Ed.* **2003**, *42*, 4923.

(10) Armentrout, P. B.; Halle, L. F.; Beauchamp, J. L. *J. Chem. Phys.* **1982**, *76*, 2449.

(11) Koyanagi, G. K.; Lavrov, V. V.; Baranov, V. I.; Bandura, D.; Tanner, S. D.; McLaren, J. W.; Bohme, D. K. *Int. J. Mass Spectrom.* **2000**, *194*, L1.

(12) See, for example, Rosenzweig, A. C. *Nat. Struct. Biol.* **2000**, *7*, 169.

(13) (a) Guzman-Vargas, A.; Delahay, G.; Coq, B. *Appl. Catal., B* **2003**, *42*, 369. (b) *Interfacial Applications in Environmental Engineering*; Schoonmaker, S. J., Keane, M. A., Eds.; Marcel Dekker Inc.: New York, 2003.

(14) (a) Moore, C. E. *Atomic Energy Levels as Derived from the Analyses of Optical Spectra*; U.S. National Bureau of Standards: Washington, 1971. (b) Martin, W. C.; Fuhr, J. R.; Kelleher, D. E.; Musgrove, A.; Podobedova, L.; Reader, J.; Saloman, E. B.; Sansonetti, C. J.; Wiese, W. L.; Mohr, P. J.; Olsen, K. *NIST Atomic Spectra Database*, version 2.0 (1999), (online); National Institute of Standards and Technology: Gaithersburg, MD available at http://physics.nist.gov/asd (March 30, 2004). (c) Van Kleef, Th. A. M.; Metsch, B. C. *Physica* **1978**, *C 95*, 251.

(15) Condon, E. U.; Shortley G. H. *The Theory of Atomic Spectra*; Cambridge University Press: London, 1963; pp 236−237.

(16) Garstang R. H. *Mon. Not. R. Astron. Soc.* **1962**, *124*, 321.

(17) Zhang, X.-G.; Armentrout, P. B. *J. Phys. Chem. A* **2003**, *107*, 8904.

(18) Schröder, D.; Schwarz, H.; Shaik, S. *Structure and Bonding*; Springer-Verlag: Berlin, Heidelberg, 2000; Vol. 97, pp 91−122.

(19) Freiser, B. S., Ed. *Organometallic Ion Chemistry*; Kluwer: Dordrecht, 1996.

(20) Sievers, M. R.; Chen, Y.-M.; Armentrout, P. B. *J. Chem. Phys.* **1996**, *105*, 6322.

(21) Chen, Y.-M.; Armentrout, P. B. *J. Chem. Phys.* **1995**, *103*, 618.

(22) Clemmer, D. E.; Dalleska, N. F.; Armentrout, P. B. *Chem. Phys. Lett.* **1992**, *190*, 259.

(23) Blagojevic, V.; Lavrov, V. V.; Orlova, G.; Bohme, D. K. *Chem. Phys. Lett.* **2004**, *389*, 303.

(24) Beyer, M. Dissertation, Technical University München, 1966.

(25) Irikura, K. K.; Beauchamp, J. L. *J. Am. Chem. Soc.* **1989**, *111*, 75.

(26) Pavlov, M.; Blomberg, M. R. A.; Siegbahn, P. E. M.; Wesendrup, R.; Heinemann, C.; Schwarz, H. *J. Phys. Chem. A* **1997**, *101*, 1567.

(27) Petrie, S. Department of Chemistry, Australian National University, Canberra, ACT 0200, Australia. Private communications. These values were calculated using the QCISD(T)/6-311+G(3df) method; the value for OA-(Se^+) does not include a spin−orbit correction.

(28) Stearns C. A.; Kohl, F. J. *High Temp. Sci.* **1970**, *2*, 146.

(29) Farber, M.; Srivastava, R. D. *J. Chem. Soc., Faraday Trans. 1* **1973**, *69*, 390.

(30) Gingerich, K. A. *J. Chem. Phys.* **1968**, *49*, 14.

(31) Kohl, F. J.; Stearns, C. A. *J. Phys. Chem.* **1974**, *78*, 273.

(32) Gingerich, K. A. *J. Chem. Phys.* **1968**, *49*, 19.

(33) Clemmer, D. E.; Sunderlin, L. S.; Armentrout, P. B. *J. Phys. Chem.* **1990**, *94*, 3008.

(34) Clemmer, D. E.; Sunderlin, L. S.; Armentrout, P. B. *J. Phys. Chem.* **1990**, *94*, 208.

(35) Kunze, K. L.; Harrison, J. F. *J. Phys. Chem.* **1989**, *93*, 2983.

(36) Berces, A.; Mitchell, S. A.; Zgierski, M. Z. *J. Phys. Chem. A* **1998**, *102*, 6340.

(37) (a) Su, T.; Chesnavich, W. J. *J. Chem. Phys.* **1982**, *76*, 5183. (b) Orcutt, R. H.; Cole, R. H. *J. Chem. Phys.* **1967**, *46*, 697. (c) Shulman, R. G.; Dailey, B. P.; Townes, C. H. *Phys. Rev.* **1950**, *78*, 145.

(38) Ryan, M. F.; Stöckigt, D.; Schwarz, H. *J. Am. Chem. Soc.* **1994**, *116*, 9565.

(39) Armentrout, P. B.; Halle, L. F.; Beauchamp, J. L. *J. Chem. Phys.* **1982**, *76*, 2449.

(40) (a) Kretschmar, I.; Fiedler, A.; Harvey, J. N.; Schröder, D.; Schwarz, H. *J. Phys. Chem. A* **1997**, *101*, 6252. (b) Kretschmar, I. Ph.D. Dissertation, Shaker Verlag, Berlin, 1999.

(41) See, for example, Shuler, K. E. *J. Chem. Phys.* **1953**, *21*, 624.

(42) Marquez, A.; Capitan, M. J.; Odriozola, J. A.; Sanz, J. F. *Int. J. Quantum Chem.* **1994**, *52*, 1329.

(43) Van Zee, R. J.; Li, S.; Weltner, W. *Chem. Phys. Lett.* **1994**, *217*, 381.

(44) Dyke, J. M.; Ellis, A. M., Feher, M.; Morris, A.; Paul, A. J.; Stevens, J. C. H. *J. Chem. Soc., Faraday Trans. 2* **1987**, *83*, 1555.

(45) Heinemann, C.; Koch, W.; Schwarz, H. *Chem. Phys. Lett.* **1995**, *245*, 509.

(46) Frisch, M. J.; Trucks, G. W.; Schlegel, H. B.; Scuseria, G. E.; Robb, M. A.; Cheeseman, J. R.; Zakrzewski, V. G.; Montgomery, J. A., Jr.; Stratmann, R. E.; Burant, J. C.; Dapprich, S.; Millam, J. M.; Daniels, A. D.; Kudin, K. N.; Strain, M. C.; Farkas, O.; Tomasi, J.; Barone, V.; Cossi, M.; Cammi, R.; Mennucci, B.; Pomelli, C.; Adamo, C.; Clifford, S.; Ochterski, J.; Petersson, G. A.; Ayala, P. Y.; Cui, Q.; Morokuma, K.; Malick, D. K.; Rabuck, A. D.; Raghavachari, K.; Foresman, J. B.; Cioslowski, J.; Ortiz, J. V.; Stefanov, B. B.; Liu, G.; Liashenko, A.; Piskorz, P.; Komaromi, I.; Gomperts, R.; Martin, R. L.; Fox, D. J.; Keith, T.; Al-Laham, M. A.; Peng, C. Y.; Nanayakkara, A.; Gonzalez, C.; Challacombe, M.; Gill, P. M. W.; Johnson, B. G.; Chen, W.; Wong, M. W.; Andres, J. L.; Head-Gordon, M.; Replogle, E. S.; Pople, J. A. *Gaussian 98*, revision A.11; Gaussian, Inc.: Pittsburgh, PA, 1998.

(47) (a) Becke, A. D. *J. Chem. Phys.* **1993**, *98*, 5648. (b) Lee, C.; Yang, W.; Parr, R. G. *Phys. Rev. B* **1988**, *37*, 785.

(48) (a) McLean, A. D.; Chandler, G. S. *J. Chem. Phys.* **1980**, *72*, 5639. (b) Krishnan, R.; Binkley, J. S.; Seeger, R.; Pople, J. A. *J. Chem. Phys.* **1980**, *72*, 650.

(49) Dolg, M.; Stoll, H.; Savin, A.; Preuss, H. *Theor. Chim. Acta* **1989**, *75*, 173.

(50) Dunning, T. H., Jr.; Hay, P. J. In *Modern Theoretical Chemistry*; Schaefer, H. F., III, Ed.; Plenum: New York, 1976; Vol. 3, p 1.

(51) (a) Schröder, D.; Fielder, A.; Ryan, M. F.; Schwarz, H. *J. Phys. Chem.* **1994**, *98*, 68. (b) Ryan, M. F.; Fielder, A.; Schröder, D.; Schwarz, H. *Organometallics* **1994**, *13*, 4072. (c) Clemmer, D. E.; Chen, Y.-M.; Khan, F. A.; Armentrout, P. B. *J. Phys. Chem.* **1994**, *98*, 6522. (d) Chen, Y.-M.; Clemmer, D. E.; Armetrout, P. B. *J. Am. Chem. Soc.* **1994**, *116*, 7815. (e) Fiedler, A.; Schröder, D.; Shaik, S.; Schwarz, H. *J. Am. Chem. Soc.* **1994**, *116*, 10734.

(52) (a) Shaik, S.; Danovich, D.; Fiedler, A.; Schröder, D.; Schwarz, H. *Helv. Chim. Acta* **1995,** *78*, 1393. (b) Danovich, D.; Shaik, S. *J. Am. Chem. Soc.* **1997**, *119*, 1773. (c) Filatov, M.; Shaik, S. *J. Phys. Chem. A* **1998**, *102*, 3835.

(53) Heinemann, C.; Schwarz, H. *Chem. Eur. J.* **1995**, *1*, 7−11.

(54) Rodgers, M. T.; Walker, B.; Armentrout, P. B. *Int. J. Mass Spectrom.* **1999**, *182/183*, 99−120.

(55) Bellert, D.; Buthelezi, T.; Lewis, V.; Dezfulian, K.; Brucat, P. J. *Chem. Phys. Lett.* **1995**, *240*, 495.

(56) Heinemann, C.; Schwarz, J.; Schwarz, H. *Chem. Phys. Lett.* **1995**, *247*, 611.

(57) Brönstrup, M.; Schröder, D.; Kretzschmar, I.; Schwarz, H.; Harvey, J. N. *J. Am. Chem. Soc.* **2001**, *123*, 142.

(58) Irikura, K. K.; Beauchamp, J. L. *J. Am. Chem. Soc.* **1989**, *111*, 75.

(59) Schröder, D.; Fiedler, A.; Herrmann, W. A.; Schwarz, H. *Angew. Chem., Int. Ed. Engl.* **1995**, *34*, 2517.

(60) Baranov, V. I.; Bohme, D. K. *Int. J. Mass Spectrom.* **1999**, *185/186/187*, 117.

(61) Zhang, X.-G.; Armentrout, P. B. *J. Phys. Chem. A* **2003**, *107*, 8915.